npj Quantum Information

https://doi.org/10.1038/s41534-026-01275-2

Article in Press

Fullqubit alchemist: quantum algorithm for alchemical free energy calculations

Received: 3 October 2025

Accepted: 12 May 2026

Cite this article as: Huang, P.-W., Boyd, G., Anselmetti, G.-L.R. *et al.* Fullqubit alchemist: quantum algorithm for alchemical free energy calculations. *npj Quantum Inf* (2026). https://doi.org/10.1038/s41534-026-01275-2

Po-Wei Huang, Gregory Boyd, Gian-Luca R. Anselmetti, Matthias Degroote, Nikolaj Moll, Raffaele Santagati, Michael Streif, Benjamin Ries, Daniel Marti-Dafcik, Hamza Jnane, Sophia Simon, Nathan Wiebe, Thomas R. Bromley & Bálint Koczor

Fullqubit alchemist: Quantum algorithm for alchemical free energy calculations

Po-Wei Huang,[1,2,*] Gregory Boyd,[1] Gian-Luca R. Anselmetti,[3] Matthias Degroote,[3] Nikolaj Moll,[3] Raffaele Santagati,[3] Michael Streif,[3] Benjamin Ries,[4] Daniel Marti-Dafcik,[1,5] Hamza Jnane,[1,6] Sophia Simon,[7] Nathan Wiebe,[8,9,10] Thomas R. Bromley,[1] and Bálint Koczor[1,2]

[1] *Quantum Motion, 9 Sterling Way, London N7 9HJ, United Kingdom*
[2] *Mathematical Institute, University of Oxford, Woodstock Road, Oxford OX2 6GG, United Kingdom*
[3] *Quantum Lab, Boehringer Ingelheim, 55218 Ingelheim am Rhein, Germany*
[4] *Medicinal Chemistry, Boehringer Ingelheim Pharma GmbH & Co KG, 88397 Biberach, Germany*
[5] *Physical and Theoretical Chemistry Laboratory, University of Oxford, South Parks Road, Oxford, OX1 3QZ, United Kingdom*
[6] *Department of Materials, University of Oxford, Parks Road, Oxford OX1 3PH, United Kingdom*
[7] *Department of Physics, University of Toronto, Canada*
[8] *Department of Computer Science, University of Toronto, Canada*
[9] *Pacific Northwest National Laboratory, Richland WA, USA*
[10] *Canadian Institute for Advanced Studies, Toronto, Canada*

(Dated: January 30, 2026)

ABSTRACT

Accurately computing the free energies of biological processes is a cornerstone of computer-aided drug design, but it is a daunting task. The need to sample vast conformational spaces and account for entropic contributions makes the estimation of binding free energies very expensive. While classical methods, such as thermodynamic integration and alchemical free energy calculations, have significantly contributed to reducing computational costs, they still face limitations in terms of efficiency and scalability. We tackle this through a quantum algorithm for the estimation of free energy differences by adapting the existing Liouvillian approach and introducing several key algorithmic improvements. We directly implement the Liouvillian operator and provide an efficient description of electronic forces acting on both nuclear and electronic particles on the quantum ground state potential energy surface. This leads to super-polynomial runtime scaling improvements in the precision of our Liouvillian simulation approach and quadratic improvements in the scaling with the number of particles relative to prior quantum algorithms. Second, our algorithm calculates free energy differences via a fully quantum implementation of thermodynamic integration and alchemy, thereby foregoing expensive entropy estimation subroutines used in prior works. Our results open new avenues towards the application of quantum computers in drug discovery.

I. INTRODUCTION

Biological processes occur in warm, aqueous environments where molecules are in constant thermal motion. Rather than adopting a single geometry, molecules in the human body continuously explore a large ensemble of configurations. As a result, thermodynamic properties such as entropy or free energy depend on the statistical distribution of a vast number of accessible conformations. Accurately estimating these properties *in silico* requires sampling this high-dimensional configuration space, which is very computationally intensive.

Modern computer-aided drug design pipelines rely heavily on the determination of thermodynamic quantities. In particular, the binding free energy between a ligand and its biological target is a key metric for ranking drug candidates[1]. Significant advancements in this field have been driven by two key factors: the exponential growth in computational power — consistent with Moore's law and the rise of parallel computing architectures — and the development of sophisticated algorithms and various protocols for free energy estimation[2].

Free energy calculations focus primarily on calculating relative binding free energies, which quantify the change in free energy between two different molecular ensembles[3–5]. Thus, in such calculations, instead of evaluating two absolute binding free energies independently, one computes their difference directly. Alchemical free energy methods accomplish this by introducing a continuous, nonphysical transformation from one chemical species into another through a pathway of fictitious intermediary states[6], drawing parallels with transforming elements in the art of alchemy. The main benefit is that because free energy is a state function, the actual physical binding process does not need to be simulated. This flexibility avoids the need to model complex kinetic mechanisms and enables more efficient estimation of free energy differences. Furthermore, for condensed-phase systems such as liquids and solids — typical in drug design — the Gibbs free energy difference can be accurately approximated by the Helmholtz free energy, as the pressure-volume work is negligible under the nearly incompressible conditions of these

* Corresponding author: Po-Wei Huang
(po-wei.huang@maths.ox.ac.uk)

phases[7,8]. Among the most widely used techniques to estimate the Gibbs free energy differences via Helmholtz free energy differences are thermodynamic integration[9] and free energy perturbation[10,11], both of which rely on sampling equilibrium ensembles on classical computers.

Among the available techniques for sampling the configuration space, molecular dynamics is one of the most widely used[3,12]. It is routinely employed in academic and industrial settings to compute thermodynamic properties from first principles[13]. However, the efficiency of free energy calculations remains a considerable challenge due to the inherent complexity of accurately capturing entropic contributions to the free energy. Reliable sampling of conformational spaces, particularly in systems with high entropic barriers, requires substantial computational resources and robust statistical mechanical frameworks[1,14].

To address some of these computational bottlenecks, the efficient simulation of molecular and quantum systems on quantum computers has emerged as a promising avenue[15–18]. Quantum simulation techniques have already shown significant improvements in runtime for calculating ground state energies of systems of correlated electrons, with potential applications spanning catalysis, materials science, and drug design[19–24].

Molecular dynamics requires simulating both electronic and nuclear degrees of freedom. In many practical cases, including most drug-like molecules, it is appropriate to treat the nuclei classically while modeling the electrons quantum mechanically, with the nuclei evolving under forces generated by the electrons[25]. Recognizing that the main bottleneck in classical computing lies in the electronic structure calculations, earlier work proposed a hybrid computational paradigm: use a quantum computer to compute electronic forces and then propagate the nuclei according to Newton's equations of motion on a classical computer[26–28]. While this is a natural way of enhancing existing classical simulation pipelines with quantum computers, the approach is fundamentally limited by measurement overhead as each electronic force must be extracted from the quantum computer via repeated measurements, a process that can take hours to days and must be repeated at each time step[24].

Recent advances extend the runtime advantages of quantum algorithms to hybrid classical–quantum dynamics, enabling a fundamental shift from the paradigm described above[29,30]. Notably, Ref.[29] introduced an approach based on the Liouvillian formalism[31] that allows the entire molecular dynamics simulation to be carried out on a quantum computer. By directly applying electronic forces to the classical nuclei via the phase kickback technique[32], it eliminates the need for repeated force measurements. When combined with quantum algorithms for estimating thermodynamic quantities[29], this framework enables the computation of free energies over exponentially large configuration spaces without relying on any classical-quantum feedback loop at every time step.

Nonetheless, these quantum algorithms still face major bottlenecks in computational efficiency. In particular, the quantum simulation method presented in Ref.[29] relies on Trotterization[33,34], which has a less favorable scaling with respect to error tolerance and evolution time than modern techniques based on block encodings[35–38]. Furthermore, the technique lacks an efficient method for calculating the differences in free energies when comparing different compounds, which is critical for end-to-end applications such as drug discovery.

In this work, we introduce a new quantum algorithm for molecular dynamics that overcomes these limitations. The algorithm relies on an improved version of the original implementation of molecular dynamics in the Liouvillian formalism presented in Ref.[29]. The latter relied on the Suzuki-Trotter product formula[33,39,40] to implement the calculation of the electronic structure and to combine the electronic and classical Liouvillians. Here, instead, we introduce a block encoding of the electronic Liouvillian, preparing ground state energy forces on a separate electronic register, and then "kicking-back" the computed values onto the nuclear registers via a form of phase kickback[32]. This enables us to implement the quantum simulation with the full (electronic and classical) Liouvillian by Hamiltonian simulation algorithms[37,41,42]. In doing so, we achieve a super-polynomial improvement in runtime scaling with respect to precision and substantially decrease the dependency on the number of particles.

We then develop a new quantum algorithm for thermodynamic integration that runs solely on the quantum computer, building on these improvements. This algorithm avoids the need for a direct entropy estimation, which can scale exponentially with the number of atoms in the simulated system[29,43]. It replaces it with internal energy estimation across interpolated molecular dynamic simulations, which can be implemented efficiently on a quantum computer and be further integrated with amplitude estimation[44] to provide additional speedups over classical methods.

Figure 1 provides an overview of our quantum algorithms: the top two rows detail the Liouvillian simulation. In addition, the bottom two rows present the computation of free energy via alchemical methods. Using the Hellmann–Feynman theorem[45,46], we construct diagonal block encodings of energy derivatives to build the Liouvillian operator, which is then used to implement its corresponding evolution operator. Combined with a block encoding of the nuclear Hamiltonian, this enables the computation of free energy differences by implementing thermodynamic integration via the Hadamard test[32,47]. A sketch of the concept behind the implementation of thermodynamic integration on a quantum computer is provided in Figure 2. Note that the controlled Liouvillian is implemented as a single operator, rather than as separate operators. A comparison of algorithmic complexities in terms of Toffoli gate counts between our work and that of Ref.[29] is presented in Table 1. For the Liouvillian simulation algorithm, we provide a super-polynomial speedup in terms of the precision ε as well as a reduction in the particle numbers N and $\tilde{N}$ by a polynomial factor. On the other hand, for the free energy calculation, we remove the dependency on the number of grid points η, which can scale exponentially with the number of qubits, as well as reduce the dependency on precision ε by a polynomial factor.

We present our algorithms in the following Results section, and we would like to ask the reader to refer to the Methods section for an introduction of the preliminaries of our methods.

II. RESULTS

A. Improved quantum algorithm for Liouvillian simulation

We provide an algorithm that utilizes evolution under the Liouvillian directly by implementing the block encoding of the electronic Liouvillian from Ref.[29]. We then encode the ground state energy derivative on an electronic register and exploit a form of phase kickback[32] to report the results to the nuclear registers. This allows us to add together the classical and electronic Liouvillians, which we then exponentiate via QSVT (in the same way one would perform Hamiltonian simulation). The benefits of our approach are the following:

1. We achieve super-polynomial asymptotic reductions of the runtime in terms of precision ε from $\mathcal{O}(\varepsilon^{-o(1)})$ in the simulation relative to the quantum algorithm in Ref.[29] to $\mathcal{O}(\text{poly}\log\frac{1}{\varepsilon})$.
2. We decrease the dependency on the number of particles by order of $\tilde{\mathcal{O}}(N^{1+o(1)}\tilde{N}^{1+o(1)}N_{\text{tot}}^{o(1)})$ and time by an order of $\tilde{\mathcal{O}}(t^{o(1)})$ from the removal of Trotterization and from the direct implementation of energy derivatives when compared to Ref.[29].

These advantages are informally summarized in the following theorem, while the formal statement (Theorem S3.6) and proof of this theorem are detailed in Supplementary Information 3.

Theorem 1 (Born-Oppenheimer Liouvillian simulation of coupled quantum-classical dynamics; informal). *Given an initial state $|\rho_0\rangle$ that encodes the initial discretized phase-space density and a discretized Liouvillian L under the NVT canonical ensemble, we can construct an explicit quantum algorithm that outputs a quantum state that is ε-close in ℓ_2 distance to $|\rho_t\rangle = e^{-iLt}|\rho_0\rangle$ using*

$$\tilde{\mathcal{O}}\left(\frac{N\tilde{N}N_{\text{tot}}^3 t}{\delta\gamma}\log^3\frac{1}{\varepsilon}\right)$$

Toffoli gates,

$$\tilde{\mathcal{O}}\left(\frac{1}{\delta}\left(NN_{\text{tot}}t + \log\frac{1}{\gamma\varepsilon}\right)\right)$$

queries to the approximate ground state preparation oracle U_I, and $\tilde{\mathcal{O}}(N_{\text{tot}} + \log\frac{t}{\delta\gamma\varepsilon})$ qubits, where N is the number of nuclei, $\tilde{N}$ is the number of electrons, $N_{\text{tot}} = N + \tilde{N}$ is the total number of particles, δ is the lower bound for the overlap between the approximate and true ground state prepared by U_I and γ is a lower bound on the spectral gap of the electronic Hamiltonian over all nuclear phase-space grid points.

Let us now detail the steps in the construction of the algorithm, which is given above as Algorithm 1. What is required is to prepare the block encoding of the Liouvillian, which can be obtained by computing partial derivatives of the extended nuclear Hamiltonian H_{ext} (inclusive of nuclear kinetic, nuclear potential, ground state energy terms, and bath terms) of the system on both position and momentum as shown in Equation (16). Once we have the block encoding of the Liouvillian, given that it remains self-adjoint, we can utilize a Hamiltonian simulation algorithm[41,42] to obtain its corresponding evolution operator and apply it to evolve a prepared initial state $|\rho\rangle$ encoding the system's initial phase-space density.

We start with the block encoding of the electronic forces, which is found to be the derivative of the ground state energy function over nuclear positions:

$$D_{n,j}^{\text{el}} := \frac{\partial E_{\text{el}}}{\partial x_{n,j}}(\boldsymbol{x})|\bar{\boldsymbol{x}}\rangle\langle\bar{\boldsymbol{x}}|. \tag{1}$$

We make use of the Hellmann-Feynman theorem[45,46] to implement this block encoding. This theorem states that the derivative of the total energy with respect to a parameter can be found by computing an expected value of the derivative of the Hamiltonian with respect to that same parameter, such that

$$\frac{\partial E(x)}{\partial x} = \left\langle \psi(x) \,\middle|\, \frac{\partial H(x)}{\partial x} \,\middle|\, \psi(x) \right\rangle, \tag{2}$$

where $H(x)$ is a Hamiltonian dependent on the continuous parameter x, $|\psi(x)\rangle$ is an eigenstate of $H(x)$ implicitly dependent on x, and $E(x)$ is the corresponding eigenenergy/eigenvalue.

When combined with the ground state preparation algorithm by Ref.[48], one can utilize the Hellmann-Feynman theorem to encode electronic forces directly into the amplitude, eliminating the need for central finite difference schemes to approximate these values. Usage of the Hellmann-Feynman theorem was previously explored in Ref.[26] under the context of estimating the molecular forces themselves, using a quantum phase estimation[47] of the Szegedy walk unitary[49] to implement the overlap estimation algorithm[50]. These forces can then be integrated into classical MD methods by replacing subsystems that compute quantum mechanical effects. In this paper, we develop a diagonal block encoding method that encodes the molecular forces for each distinct nuclear position configuration. Rather than leveraging phase estimation to extract the forces, we utilize the Hellmann-Feynman theorem directly as a series of matrix multiplication operations, block-encoding the forces by first computing the ground state, applying the force operator, and then directly uncomputing the ground state. This block-encodes the scalar value of the forces in the top left element.

Note that in our case, even though we do not use the exact eigenstate for the Hellmann-Feynman theorem, the errors that stem from the inexact ground state, even after the ground state preparation algorithm, can be accounted for in the error analysis of the block encoding, while discretization errors can be suppressed by adding more qubits. Further, as our choice of bases from the electronic system, we also need not consider the effects of Pulay stress[51,52], given that they are absent under nuclear-position-independent bases such as plane waves. A further discussion of basis sets involving Pulay forces under the Hellmann-Feynman theorem can be found in Ref.[26].

When implemented in superposition, by applying the controlled operators above, and subsequently projecting the electronic registers into the zero state, we can encode the force values onto the nuclear registers for all different nuclear positions by phase kickback[32]. Therefore, we can implement

$$D^{\mathrm{el}}_{n,j} = \left\langle \psi_0(\boldsymbol{x}) \left| \frac{\partial H_{\mathrm{el}}(\boldsymbol{x})}{\partial x_{n,j}} \right| \psi_0(\boldsymbol{x}) \right\rangle |\bar{\boldsymbol{x}}\rangle\langle\bar{\boldsymbol{x}}|, \tag{3}$$

for the discretized grid space of position on the quantum computer. This approach results in the construction of the energy derivative operator with a logarithmic dependency on precision as shown in Lemma S3.2. Combining the results with an implementation of the discretized momentum derivative operator $D_{p'_{n,j}}$ shown in Ref.[29], this provides a block encoding of the electronic Liouvillian via linear combination of unitaries[53]:

$$\tilde{L}_{\mathrm{el}} = i \sum_{n=1}^{N} \sum_{j=1}^{3} D^{\mathrm{el}}_{n,j} \otimes D_{p'_{n,j}}. \tag{4}$$

The details of this block encoding are shown in Proposition S3.3. This further provides a logarithmic dependency on the error of the total Liouvillian simulation algorithm, as the Liouvillian is directly and analytically block-encoded.

In addition to decreasing the runtime dependency on precision, by using the Hellmann-Feynman theorem to block-encode the force operator instead of a central finite difference approximation[29], we reduce the scaling factor of the block encoding of the electronic Liouvillian by a factor of $\mathcal{O}(N_{\mathrm{tot}})$[26]. This is due to the reduced number of terms to implement in the Hellmann-Feynman approach. When combined with the classical Liouvillian, this produces a reduction in the total scaling of $\mathcal{O}(\tilde{N})$ in the full Liouvillian, with the implementation cost and details shown in the proposition below:

Proposition 2 (Block encoding of the Liouvillian; informal). *We can construct an explicit* $(\alpha_L, a_L, \varepsilon_L)$*-block-encoding of the Liouvillian* L *where*

$$\alpha_L \in \mathcal{O}\left(N N_{\mathrm{tot}}\right)$$

$$a_L \in \mathcal{O}\left(\tilde{N} + \log \frac{N_{\mathrm{tot}}}{\varepsilon_L}\right).$$

This block encoding can be prepared with $\mathcal{O}(\frac{1}{\delta})$ *queries to* U_I*, and*

$$\tilde{\mathcal{O}}\left(\frac{\tilde{N} N_{\mathrm{tot}}^2}{\delta\gamma} \log^2 \frac{1}{\varepsilon_L}\right)$$

Toffoli gates.

The formal statement (Proposition S3.5) and proof of this proposition can be found as part of the proof of Theorem 1 in Supplementary Information 3. In the context of the Liouvillian simulation algorithm, this results in a reduction in runtime by $\mathcal{O}(\tilde{N})$ in the Hamiltonian simulation step, due to the reduced scaling factor of central finite difference methods.

In addition to the runtime improvements resulting from the direct implementation of the Liouvillian and the use of the Hellmann-Feynman theorem, further speedups can be achieved. Namely, all sublinear dependencies are removed solely by using direct evolution as opposed to Trotterization. Furthermore, by directly implementing the electronic Liouvillian in superposition via LCU[53] instead of taking the product of multiple commutating controlled Hamiltonian simulations, we can effectively reduce the number of queries to the ground state preparation algorithm. This results in a further reduction of the runtime by a factor of $\mathcal{O}(N)$.

Lastly, while our results are primarily focused on the NVT canonical ensemble, these improvements can be easily translated to the NVE microcanonical ensemble by replacing the block encoding of the classical Liouvillian with its NVE counterpart in Ref.[29]. These results are shown in Supplementary Information 3 D.

B. Quantum algorithm for alchemical free energy calculation

The results we developed in the previous section give us access to a block encoding of the full Liouvillian as per Proposition 2. This allows us to implement algorithms that require access to weighted sums of Liouvillian terms. With simulations under the NVT ensemble, this enables the efficient preparation of thermal states that can be further used to compute thermal averages such as the free energy.

Prior work in Ref.[29] computes the free energy by first estimating both the internal energy and Gibbs entropy separately, which are then subtracted. While the internal energy can be efficiently estimated by the Hadamard test with the nuclear Hamiltonian, the estimation of Gibbs entropy scales with the dimension η of the density matrix $|\rho_t\rangle\langle\rho_t|$[43]. Given that $|\rho_t\rangle$ is prepared on a collection of registers $|\bar{x}_{n,j}\rangle$, $|\bar{p}'_{n,j}\rangle$, $|\bar{s}\rangle$, and $|\bar{p}_s\rangle$, the dimension η corresponds to the dimension of the classical nuclear phase-space. If an individual register has dimension g, then

$\eta \in \mathcal{O}(g^{6N+2})$ and is hence exponential to the number of atoms. However, this exponential scaling of entropy calculation may not be due to the algorithm itself, as the problem of computing absolute free energies is found to be NP-hard by reducing it to the problem of partition function computation, which is NP-complete[54].

Contrary to the computation of absolute free energies, relative free energies are known to be easier to compute, with various classical algorithms dedicated to this purpose[9,10]. Aside from the reduced computational complexity, relative free energies are more relevant to applications because they directly determine observable quantities like binding affinities and reaction equilibria[7]. Hence, in our work, we compute relative free energies instead of absolute free energies. Borrowing techniques from classical computational chemistry literature and leveraging alchemical methods described in Section IV B enables us to calculate the free energy differences between two closely related systems. With this strategy, we provide the following improvements to calculating free energy differences.

1. Compared to Ref.[29], by implementing thermodynamic integration, we bypass the use of entropy estimation algorithms[43], which scale with the total size of the nuclear phase-space η used in the simulation (unless entropy estimation is evaluated over a coarsened grid) and therefore exponentially with the number of qubits $\Theta(N)$ that are used to represent the nuclear degrees of freedom. Our algorithm is only dependent on calculating the internal energy, which can be achieved efficiently via the Hadamard test and is not dependent on η.
2. We achieve $\tilde{\mathcal{O}}\left(\frac{1}{\varepsilon}\right)$ scaling for Helmholtz free energy estimation by using the Liouvillian simulation algorithm in the previous section, as well as a more efficient block-encoding of the nuclear Hamiltonian that depend only logarithmically on the overall precision — we achieve this by replacing quantum phase estimation[47] for ground state energy computation with phase kickback[32] techniques.

Below, we state our main result:

Theorem 3 (Quantum complexity for thermodynamic integration; informal). *Given an initial state $|\rho_0\rangle$ that encodes the initial discretized phase-space density and two discretized Liouvillians, L_A, and L_B, under the NVT canonical ensemble encoding the dynamics for systems A and B, as well as an equilibration time t_{eq} for Liouvillian simulation, there exists a quantum algorithm that can compute the free energy difference between the two systems up to additive ε-precision with $1-\xi$ success probability using*

$$\tilde{\mathcal{O}}\left(\frac{N\tilde{N}N_{\mathrm{tot}}^5 t_{\mathrm{eq}}}{\delta\gamma\varepsilon}\log\frac{1}{\xi}\right)$$

Toffoli gates,

$$\tilde{\mathcal{O}}\left(\frac{NN_{\mathrm{tot}}^3 t_{\mathrm{eq}}}{\delta\varepsilon}\log^2\left(\frac{1}{\gamma}\right)\log\left(\frac{1}{\xi}\right)\right)$$

queries to the approximate ground state preparation oracle U_I, and $\tilde{\mathcal{O}}(N_{\mathrm{tot}}+\log\frac{t_{\mathrm{eq}}}{\delta\gamma\varepsilon})$ qubits, where N is the number of nuclei, $\tilde{N}$ is the number of electrons, $N_{\mathrm{tot}}=N+\tilde{N}$ is total number of particles, δ is the lower bound for the overlap on the approximate and true ground state prepared by U_I and γ is a lower bound on the spectral gap of the electronic Hamiltonian over all nuclear phase-space grid points.

The formal statement (Theorem S4.6) and proof of this proposition have been deferred to Supplementary Information 4.

We are now ready to describe the main algorithm (Algorithm 2). Suppose we want to compute the free energy differences between two systems A and B. Then, to perform thermodynamic integration over Λ in superposition, we need to apply an interpolated NVT Liouvillian L_Λ, which can be easily constructed from the Λ-dependent nuclear Hamiltonian $H_\Lambda=(1-\Lambda)H_A+\Lambda H_B$ as the Liouvillian is linearly dependent on the Hamiltonian as seen in Equation (16). Given this linearity, the corresponding Liouvillian is $L_\Lambda=(1-\Lambda)L_A+\Lambda L_B$, where L_A and L_B may act on different sets of nuclear registers. Registers describing nuclear degrees of freedom that are shared between A and B can be acted on by both L_A and L_B, or only one of them (if there is an increase or decrease of nuclei). Given this construction of the intermediate Liouvillian via LCU, we do not actually construct individual components of the intermediate Liouvillians and hence do not need to formulate the nuclear Hamiltonian H_Λ and ground state correction terms $E_{\mathrm{el},\Lambda}$ for the intermediate systems. This implies that the assumptions on ground state overlap δ and spectral gap γ only apply to the physical initial and final systems A and B.

To compute the free energy, starting with a common initial state $|\rho_0\rangle$, for each Λ, we evolve the state by the interpolated NVT Liouvillian L_Λ over a predetermined and sufficient equilibration time t_{eq} such that we obtain the thermal state $|\rho_\Lambda\rangle=e^{-iL_\Lambda t_{\mathrm{eq}}}|\rho_0\rangle$. Given that the state includes registers corresponding to the heat bath, we then trace out the bath registers in a quantum analog of integrating over them to obtain $\rho_{\mathrm{sys},\Lambda}=\mathrm{Tr}_{\mathrm{bath}}(e^{-iL_\Lambda t_{\mathrm{eq}}}|\rho_0\rangle\langle\rho_0|e^{iL_\Lambda t_{\mathrm{eq}}})$. By the thermodynamic integration algorithm, we can then compute the free energy difference between the systems A and B by computing

$$\Delta\tilde{F}=\frac{1}{N_\Lambda}\sum_\Lambda \mathrm{Tr}(\rho_{\mathrm{sys},\Lambda}(H_B-H_A))$$
$$=\frac{1}{N_\Lambda}\sum_\Lambda \langle\rho_\Lambda|\,(H_B-H_A)\otimes\mathbb{I}\,|\rho_\Lambda\rangle \tag{5}$$

This quantity can be computed on a quantum computer via the Hadamard test[32,47], where we first create a uniform superposition over N_Λ points with the unitary $\textsc{Prep}_\Lambda$, apply time evolution with L_Λ, and a final application of a controlled block encoding of the nuclear Hamiltonian difference H_B-H_A. We show an illustration of the quantum circuit in Figure 3.

Delving further into the implementation details, we first discuss the implementation of the evolution of Λ-controlled Liouvillians. From the results of Proposition 2, we can produce block encodings of the Liouvillians L_A and L_B, but with different scaling factors α_{L_A} and α_{L_B}. We block-encode the interpolated Liouvillian L_Λ by a weighted LCU whose weights are dependent on α_{L_A}, α_{L_B}, and Λ, which has a scaling factor of

$$\alpha_\Lambda = (1-\Lambda)\alpha_{L_A} + \Lambda\alpha_{L_B} \tag{6}$$

To perform the Hamiltonian simulation by QSVT, the polynomial approximations of $e^{-iL_\Lambda t_{\text{eq}}}$ will also depend on Λ as the number of queries to U_{L_Λ} is dependent on α_Λ. We provide two strategies to perform this transformation of L_Λ, first using standard QSVT, and then an approach using QSVT without angle finding[55] that provides the $\mathcal{O}(\frac{1}{\varepsilon})$ scaling of our algorithm.

Firstly, under conventional QSVT schemes, for each Λ in superposition, we require calculation of the phase angles $\{\theta_\Lambda\}$ with either analytical methods, or with optimization methods[56–58], where the scaling of the number of Λ-s required, or N_Λ, can be shown to be

$$N_\Lambda \in \mathcal{O}\left(\frac{\|L_A - L_B\|\|H_A - H_B\|t_{\text{eq}}}{\varepsilon}\right), \tag{7}$$

by bounding left Riemann sum errors and where a proof is presented in Supplementary Information 4 A. The QSVT sequence must have a length sufficient for the largest polynomial degree required for any Λ. For other values of Λ, the final angles can be set to 0 such that the remaining applications of U_{L_Λ} and its inverse create the identity. In the case of optimization methods, one can set the degree of optimization $\mathcal{D}$ directly to the maximum degree. If the angles are classically loaded, then we need an extra $\mathcal{O}(N_\Lambda)$ arbitrary rotation gates to load all required phase angles per query of U_{L_Λ}, as we need a different phase gate for each Λ.

However, one can bypass this by implementing the classical computations on a separate quantum register in superposition and then loading the results directly into the phase angles, which would then cost at most $\mathcal{O}(\text{poly}\,\mathcal{D}\,\text{poly}\log N_\Lambda)$ additional gates to load the phase angles. Furthermore, suppose we replace the QSVT procedure with generalized quantum signal processing (GQSP)[59]. In that case, it is known that the classical algorithm for computing the phase angles scales as $\mathcal{O}(\mathcal{D}\log\mathcal{D})$. Thus, when implemented on a quantum computer, we expect the number of gates to be at most $\tilde{\mathcal{O}}(\mathcal{D}\,\text{poly}\log N_\Lambda)$. However, the precise scaling of such algorithms when implemented on quantum computers, as well as the quantum circuit for such implementations, is not obvious.

An alternative method sidesteps the requirement of angle finding by using recent results on QSVT without classical angle finding[55] by instead encoding a functional representation in a diagonal block encoding, in this case with entries $\exp(-it\alpha_\Lambda \cos\frac{2\pi k}{4\mathcal{D}})$ for $k \in [4\mathcal{D}]$, where $\mathcal{D} \in \mathcal{O}(\max(\alpha_{L_A}, \alpha_{L_B})t_{\text{eq}} + \log\frac{1}{\varepsilon})$ is the polynomial approximation degree. Such function entries are computed in superposition via quantum arithmetic circuits[60] while controlled on Λ. This can then be encoded into the amplitude of the diagonal block encoding via controlled rotations or the alternating-sign trick[61]. The reason that the additional cosine in the function is needed is due to the use of qubitized operators, whose eigenvalues are arccos of the original block encoded matrix. This method allows for a gate count scaling $\mathcal{O}(\log^2 N_\Lambda)$ to implement the function representation. Adding the additional $\mathcal{O}(\log^2 N_\Lambda)$ cost to produce the weighted Liouvillian per query to U_{L_Λ}, this requires an additional $\mathcal{O}(\mathcal{D}\log^2 N_\Lambda)$ gates for implementation. On the other hand, this method requires an additional constant factor calls to the block encoding of the interpolated Liouvillians U_{L_Λ} as well as more ancilla qubits when compared to standard QSVT/GQSP. However, it bypasses the requirement of implementing phase angle finding algorithms on a quantum computer, as needed for standard QSVT/GQSP implementations. A more detailed discussion of an exact construction is provided in Supplementary Information 4 B.

We note that while the dependency on N_Λ is logarithmic in the runtime, this does not indicate an exponential speedup when compared to classical methods. While conventional thermodynamic integration implementations would evaluate the different N_Λ interpolated systems individually and obtain the free energy via numerical integration methods such as Simpson's rule or specifically designed physics-based fitting functions[62] for higher accuracy, Monte Carlo integration[63] can be applied to obtain faster runtime asymptotics. The number of samples in Monte Carlo integration would then depend on the square of the spectral norm of the nuclear Hamiltonian difference ΔH as opposed to N_Λ, for which the runtime is at most logarithmically dependent on the Monte Carlo integration. This logarithmic dependency stems from the precision of floating point representation on classical computers, it being $\mathcal{O}(N_\Lambda^{-1})$.

Moving on from the implementation of interpolated Liouvillians, one then time evolves the system for a duration t_{eq} that is sufficient to equilibrate all N_Λ Liouvillians $\{L_\Lambda\}$ such that their corresponding phase-space densities ρ_Λ serve as classical thermal distributions. We then obtain the state

$$\frac{1}{\sqrt{N_\Lambda}}\sum_\Lambda |\Lambda\rangle\,|\rho_\Lambda\rangle\ , \tag{8}$$

where $|\rho_\Lambda\rangle$ is the state of the nuclear and environmental degrees of freedom produced by the evolution of the Liouvillian L_Λ. Under NVT Liouvillian equilibration, the state obtained by tracing out the bath registers $|\bar{s}\rangle$ and $|\bar{p}_s\rangle$ corresponds to a thermal state of the nuclear registers. Note that the heat bath variable s should still be part of the description of the thermal state as the extended Hamiltonian with the Nosé thermostat is dependent on s. Therefore, s is required for a description of the thermal state, and will have corresponding terms in Hamiltonians

H_A and H_B to be interacted upon in the Hadamard test. Thus, we duplicate the contents of $|\bar{s}\rangle$ to a separate register by CNOT gates, which can be traced out while the original is part of the registers that the Hadamard test is applied to[29]. We refer the reader to Supplementary Information 1 for a more in-depth discussion as to why $|s\rangle$ is needed. Note that this is shown in Figure 3 as the additional CNOT gate from the $|\bar{s}\rangle$ to the $|0\rangle_s$ register.

To obtain the nuclear Hamiltonian differences $\Delta H = H_B - H_A$, we take block encodings of the nuclear Hamiltonian for both systems A and B, where for each system, we have

$$H_{\text{nuc}} = H_{\text{kin}} + H_{\text{pot}} + H_{\text{gse}}\,, \tag{9}$$

where the three terms correspond to diagonal block encodings of the values of the kinetic, potential, and ground state Hamiltonian of the relevant points in phase-space, respectively. While the kinetic and potential energy terms are previously efficiently implemented in Ref.[29], we draw attention to the implementation of H_{gse}, which we achieve by preparing the electronic ground state for each point in the discretized grid space for position and applying a block encoding of the electronic Hamiltonian H_{el} before uncomputing the ground states such that

$$\begin{aligned} H_{\text{gse}} &= \sum_{\bar{\boldsymbol{x}}} E_{\text{el}}(\boldsymbol{x}) |\bar{\boldsymbol{x}}\rangle\langle\bar{\boldsymbol{x}}| \\ &= \sum_{\bar{\boldsymbol{x}}} \langle\psi_0(\boldsymbol{x})|H_{\text{el}}(\boldsymbol{x})|\psi_0(\boldsymbol{x})\rangle\, |\bar{\boldsymbol{x}}\rangle\langle\bar{\boldsymbol{x}}|\,. \end{aligned} \tag{10}$$

This encodes the ground state energy in the main nuclear registers by phase kickback in a similar fashion to our implementation of encoding electronic forces in Section II A. This approach to implementing H_{gse} eliminates the use of phase estimation, as shown in previous approaches[29], and reduces the runtime dependency on precision to a logarithmic scaling.

The difference in energies is then implemented by taking the difference between the block encoding of H_A and H_B via the LCU approach. Here, thermodynamic integration requires the assumption that systems A and B have a relatively high overlap in their nuclear phase spaces, and thus, most kinetic and potential Hamiltonian terms can be expected to cancel each other out. However, this is not the case for the ground state energy of the electronic Hamiltonians due to the separate ground state preparations for systems A and B, and would still have a scaling factor of $\mathcal{O}(\tilde{N}N_{\text{tot}})$.

In the following result, we construct the difference via LCU for simplicity, while noting that in practice, the block encoding implementation can be made more efficient and with a lower scaling factor.

PROPOSITION 4 (Block encoding of the nuclear Hamiltonian; informal). *We can explicit construct a $(\alpha_H, a_H, \varepsilon_H)$-block-encoding of the nuclear Hamiltonian H_{nuc} where*

$$\alpha_H \in \mathcal{O}\left(N_{\text{tot}}^2\right)$$

$$a_H \in \mathcal{O}\left(\tilde{N} + \log\frac{N_{\text{tot}}}{\varepsilon_{\text{nuc}}}\right)$$

can be prepared using $\mathcal{O}(\frac{1}{\delta})$ queries to U_I, and

$$\tilde{\mathcal{O}}\left(\frac{\tilde{N}N_{\text{tot}}^2}{\delta\gamma}\log^2\left(\frac{1}{\varepsilon_{\text{nuc}}}\right)\right)$$

Toffoli gates.

The formal statement (Proposition S4.5) and proof of this proposition can be found in Supplementary Information 4 C. Using our results above, we can block-encode $\Delta H = H_B - H_A$ via LCU with a worst-case scaling factor of $\alpha_{H_A} + \alpha_{H_B}$. However, in practice, it may often be beneficial to block encode the difference between the two operators separately.

Given this block encoding, we extract the free energy value using the Hadamard test. The probability of measuring the $|0\rangle$ state on the Hadamard test ancilla register is

$$\begin{aligned} \mathbb{P}_{\Delta\tilde{F}} &= \frac{1}{2N_\Lambda}\sum_\Lambda \left(\operatorname{Re}\langle\rho_\Lambda|\,U_\Delta\,|\rho_\Lambda\rangle + 1\right) \\ &= \frac{1}{2N_\Lambda}\sum_\Lambda \left(\frac{\langle H_B - H_A\rangle_\Lambda}{\alpha_\Delta} + 1\right) \\ &= \frac{1}{2}\left(\frac{\Delta\tilde{F}}{\alpha_\Delta} + 1\right)\,, \end{aligned} \tag{11}$$

giving us the value of the free energy difference. Then, instead of directly measuring the $|0\rangle$ state, we can use amplitude estimation[44] on the result of the Hadamard test. We can obtain the estimation of $\Delta\tilde{F}$ up to ε-precision by $\mathcal{O}(\frac{\alpha_{H_A}+\alpha_{H_B}}{\varepsilon})$ queries to the full Hadamard test circuit. We can treat the superposed Liouvillian simulations as quantum sampling access over the Λ-dependent classical thermal states. Thus, our approach achieves a scaling in terms of the precision ε that is quadratically better than a classical thermodynamic integration modified to utilize Monte Carlo integration[64] without considering potential improvements from implementing MD simulations on quantum computers as mentioned in Section II A.

III. DISCUSSION

We present a quantum algorithm for simulating molecular dynamics based on the Liouvillian formalism of classical mechanics that achieves a super-polynomial improvement in the precision scaling over prior quantum algorithms. We then apply this improved algorithm to develop an efficient quantum algorithm for computing free energy differences via alchemical methods.

While previous work[29] treated the electronic and classical Liouvillians separately, here we introduce an efficient block encoding of the full (electronic + classical) Liouvillian. Our block encoding relies on phase kickback techniques to directly transfer forces and energies computed on electronic registers to the nuclear registers and therefore removes the need for phase estimation[47] to obtain electronic forces[26], or the need for Trotterization to interleave separate classical and electronic Liouvillian evolutions[29]. This block encoding can then be used in a Hamiltonian simulation algorithm to provide a super-polynomial improvement in the scaling of the runtime of hybrid quantum-classical molecular dynamics with respect to the precision. Furthermore, by utilizing the Hellmann-Feynman theorem[45,46] and direct block encodings of electronic force operators[26], we significantly decrease the dependency of the runtime on the number of particles compared to central finite difference methods. For a more detailed comparison that includes a breakdown of subroutines, please refer to Supplementary Tables 2 and 3 in Supplementary Information 4.

Our fundamentally improved Liouvillian simulation then enables us to develop a quantum algorithm for alchemical free energy calculation that achieves a $\tilde{\mathcal{O}}(\frac{1}{\varepsilon})$ scaling with respect to precision. Our alchemical approach is a key enabler as it forgoes fundamentally more expensive entropy estimation, whose runtime on a quantum computer scales exponentially with the number of qubits representing the nuclear registers — and hence with the number of atoms — due to the exponential growth of the phase-space with the number of particles[29,43]. Specifically, we use thermodynamic integration[3,9] to compute the free energy difference between two molecular ensembles directly. This is achieved by defining a thermodynamic path connecting two ensembles and integrating over the change of internal energy along the path.

Our approach performs this numerical integration coherently on a quantum computer: we simulate molecular dynamics at each interpolation point along the path by coherently evolving a superposition of phase-space densities, each under a distinct Liouvillian. A key algorithmic development here is that we construct methods to apply different polynomial transformations in superposition using both standard QSVT/GQSP as well as QSP without angle finding[55], enabling efficient application of different transformations tailored to each block-encoded Liouvillian on the thermodynamic path. Finally, we extract the free energy difference via the Hadamard test followed by amplitude estimation. The gate overhead for this superposition of Liouvillian dynamics is only polylogarithmic in the number of interpolation points that discretize the thermodynamic path.

Our approach can, in theory, provide exponential advantage relative to known classical methods with provable guarantees, such as full configuration interaction (FCI)[65], for computing free-energy differences under the assumption that an oracle can be constructed that prepares a surrogate ground state with polynomial overlap with the ground state at every point in the thermodynamic integration and that the mixing time is polynomial. Examples of families of fermionic Hamiltonians where the ground state can be efficiently prepared can be found in Ref.[66], where it is shown that their ground state can encode the output of an arbitrary quantum circuit.

We briefly compare our methods with hybrid quantum–classical approaches that replace electronic-structure calculations with quantum primitives such as phase estimation[26,28]. First, we discuss the number of classical iterations and thus, the number of times we need to query the quantum computer for electronic structure calculations. We note that the classical molecular dynamics, at best, scales as $\mathcal{O}(\varepsilon^{-o(1)})$ in the number of time steps required. MD solves Newton's equations iteratively, updating particle positions and momenta each timestep[3,12], and estimates phase-space densities via long-time averages assuming ergodic exploration. A common method used for MD is Verlet integration[67], a second-order symplectic method with global trajectory error step count $\mathcal{O}(1/\sqrt{\varepsilon})$ to achieve final error ε. Under the Liouvillian formalism and Suzuki–Trotter viewpoint, this induces the same error order in the phase-space density[68], paralleling Ref.[29]. Higher-order symplectic integrators[69] can reduce the error such that the runtime required is $\mathcal{O}(\varepsilon^{-1/q})$ for some q, though such methods are rarely used in practice.

Second, hybrid algorithms typically require fewer qubits and shorter circuit depths, given only the computation of the electronic structure problem solved with the quantum computer. However, reading out classical information at each timestep is necessary, which incurred a cost of $\mathcal{O}(\frac{1}{\varepsilon})$ per timestep via phase estimation. Combining the above runtime estimates for readout and for classical MD integration, we conclude that hybrid algorithms are likely to require a higher asymptotic runtime than our approach. Specifically, we see that we can compute free energy differences using $\tilde{\mathcal{O}}\left(\frac{N\tilde{N}N_{\mathrm{tot}}^5 t_{\mathrm{eq}}}{\delta\gamma\varepsilon}\log\frac{1}{\xi}\right)$ Toffoli gates.

To provide a sense of the amount of required quantum resources, we sketch a back-of-the-envelope estimate for the number of qubits. We consider a 20-atom molecule with 200 electrons and calculate the number of qubits required in the main nuclear and electronic registers. We assume coordinates of all nuclear degrees of freedom are discretized into $g = 2^{12}$ grid points (i.e., 12 qubits per nuclear degree of freedom). Therefore, representing all nuclear degrees of freedom requires approximately 1500 logical qubits, given each atom has 6 degrees of freedom (three position and three momentum), and that we also account for bath registers.

We further assume the wave function of each electronic degree of freedom is represented using $B = 2^{15}$ plane waves (i.e., 15 qubits per electron and coordinate). Therefore, a total of $15 \times 3 \times 200 = 9000$ logical qubits are required to represent all electrons. Including the negligible number of ancilla qubits (which are logarithmically bounded), we estimate that the number of logical qubits is on the order of ten thousand even for a small system – this is likely beyond the capabilities of early fault-tolerant machines, however, reasonably within reach for realistic and mature quantum computers. On the other hand, the significant advantage of our approach is that scaling up the number of particles only requires a proportionally increased number of logical qubits.

Let us note, however, that estimating the number of required Toffoli gates is significantly more involved, given resource estimates typically report upper bounds, and we expect our bounds are loose – however, it is beyond the scope of the present work to optimize our approach for explicit implementations.

Though our algorithms may be able to provide asymptotic speedups against hybrid quantum-classical methods and classical algorithms with provable guarantees, comparisons to well-established computational chemistry methods that have heuristic elements are much more unclear. In search for potential practical quantum advantages, the quantum algorithms presented here contain three main potential sources of asymptotic speedups over classical methods: (1) the replacement of iterative updates for MD simulation with a single evolution operator, improving on runtime dependencies of precision, (2) efficient coherent simulation of a large number of molecular dynamics trajectories for thermodynamic integration, and (3) efficient computation of the quantum dynamics of the electronic ground state and associated forces that can potentially be hard to simulate on a classical computer to guaranteed precision, where the last point is of particular value.

So far, we have not addressed the asymptotic behavior of the equilibration time t_{eq} with the error tolerance of the simulation. With completely integrable systems, the equilibration time can scale with $\mathcal{O}(\log \frac{1}{\varepsilon})$ with additional weighting over time averages[70]. However, while the Coulomb energy forces give rise to a multidimensional harmonic oscillator, an integrable system, the potential terms provided by the Born-Oppenheimer potential energy surface are generally not believed to be completely integrable (although empirical results show that this bound can be observed for some non-integrable systems[71]). It is therefore generally a challenge to bound this parameter for general systems, and such bounds may depend on the eigenstate thermalization hypothesis (ETH) when applied to open systems[72–75]. We therefore treat t_{eq} as a potentially unbounded parameter in our scaling results.

We now briefly discuss factors that may affect t_{eq}. First, properties of the energy landscape may substantially affect the equilibration time. In particularly challenging cases, the energy landscape may have deep basins of meta-stable regions where transitions between the meta-stable regions are separated by high energy barriers, which may lead to an increase in the thermalization time of classical MD, potentially by several orders of magnitude. This issue is potentially mitigated via the Liouvillian formalism that we use in the present manuscript, as we do not propagate a single configuration by Hamiltonian dynamics, but rather the phase space density instead. This alleviates some of the need for the simulation to actually "cross" the rare event threshold, but low-quality initialization of the phase space density may still lead to a significantly increased thermalization time. These challenges in our quantum algorithm may be tackled by further exploration of quantum counterparts for classical rare event processing of molecular dynamics[3], such as the Bennett-Chandler approach[76,77]. In our paper, we mainly do not consider the occurrence of rare events with meta stability, given that classical literature with methods beyond naïve molecular dynamics as well. Under such circumstances, a polynomial overall algorithmic runtime holds in regimes where the thermostat dynamics mix in polynomial equilibration time t_{eq}.

On the other hand, given our coupling of the system with a Nóse thermostat, parameters intrinsic to the thermostat can be adjusted to affect the equilibration time. In particular, the effective mass Q of the thermostat and the fixed temperature T affect terms in the extended nuclear Hamiltonian H_{ext}, and this in turn affects the eigenstates of said Hamiltonian. Per the dependency of the equilibration time on the eigenstate thermalization hypothesis, as mentioned before, we can then see that when the underlying Hamiltonian and eigenstates are altered, the amount of time to thermalize and equilibrate the system would be affected as well.

We now move on to our discussion of cases where our assumptions on the Born-Oppenheimer approximation fail, and the approach of simulating nuclei classically and electrons quantumly may not be applicable. An alternative quantum computational approach would involve representing both the nuclei and electrons as quantum particles and leveraging algorithms for the preparation of quantum thermal states[78,79], and it may be more similar in nature to Monte Carlo methods. Apart from this additional ability to operate beyond Born-Oppenheimer approximations, it would be an interesting future research direction to compare our quantum algorithm, which uses a hybrid quantum-classical representation of molecules, with such fully-quantum approaches. Currently, it is not obvious which of the algorithms would have the most favorable scaling with respect to the number of particles and whether the progress on bounds on the mixing times of Lindbladians for specific cases[80–83] would yield an asymptotic advantage over the classical equilibration times in the Liouvillian framework we use here.

Looking forward, it will be important to identify concrete scenarios where the alchemical quantum algorithm offers an absolute runtime advantage over classical methods for free energy estimation. This requires obtaining fine-grained resource estimates on systems representative of practical applications to determine constant-level overheads. Performing such an analysis will require the construction of suitable block encodings for the molecular systems as well as a quantitative examination of potential implementations of an efficient oracle for approximate ground state preparation at all points in phase-space, including SAD, extended Hückel methods, and beyond.

Another important question left open by this work is that of deciding the ultimate limits on Helmholtz free-energy estimation for quantum systems. At present, our work provides a worst-case asymptotic advantage over the results of Ref.[29], but this does not imply that the improvements that we have observed have led to the ultimate limits of free-energy estimation using thermodynamic integration. While we do not expect the dependency of precision ε and spectral gap γ to be improved due to fundamental limits — except when further structure of the problem can be assumed, the dependency on the particle number may be improved via improved representations and quantum algorithmic subroutines. In addition, a large runtime dependency on the particle number can be provided if the ground state preparation can be decoupled somehow from the time evolution, as repeated ground state preparations are the main bottleneck of our algorithm. Further, other improvements over exact computation of entropy differences[29] may be attainable using Metropolis-Hastings ideas for thermalization[63,84,85] to approximately calculate free energies. We hope that future work will continue to make progress in improving the speed, accuracy, and range of applicability of methods for estimating both Gibbs and Helmholtz free energy differences across a wide range of physical systems.

IV. METHODS

A. Molecular dynamics within the Liouvillian formalism

Simulating the time evolution of a physical system is a crucial task in physics, with numerous applications, such as molecular dynamics (MD)[3]. MD simulations are often used to evaluate ensemble properties of a physical system, which can be used to estimate macroscopic quantities such as free energies. Different ensembles can be defined. For example, the microcanonical ensemble[86], also known as NVE, is a statistical ensemble where the total number of particles (N), total volume (V), and the total energy (E) are held constant. However, for the calculation of chemically relevant properties, we require the canonical ensemble[86,87], NVT, where the system is coupled to a heat bath to ensure a constant temperature (T). When coupled to the Nosé thermostat[87,88], an extra degree of freedom s for the heat bath is introduced into the Hamiltonian.

To construct the corresponding nuclear Hamiltonian that governs the dynamics, we write out the kinetic, Coulombic, and ground state energy terms as follows:

$$H_{\mathrm{nuc}} = \sum_{n=1}^{N}\sum_{j=1}^{3}\frac{p_{n,j}^2}{2m_n} + \sum_{k=1}^{N-1}\sum_{n=k+1}^{N}\frac{Z_n Z_k}{\|x_n - x_k\|} + E_{\mathrm{el}}(\boldsymbol{x}), \tag{12}$$

Under NVT canonical simulations with the Nosé thermostat, the nuclear Hamiltonian has additional terms concerning an extra degree of freedom s that represents the heat bath that equilibrates the system to a fixed temperature T. The extended Nosé nuclear Hamiltonian governing the dynamics can thus be formulated as follows[29,87]:

$$H_{\mathrm{ext}}^{(\mathrm{NVT})} = \sum_{n=1}^{N}\sum_{j=1}^{3}\frac{p_{n,j}'^2}{2m_n s^2} + \sum_{k=1}^{N-1}\sum_{n=k+1}^{N}\frac{Z_n Z_k}{\|x_n - x_k\|} + \frac{p_s^2}{2Q} + N_f k_B T\ln(s) + E_{\mathrm{el}}(\boldsymbol{x}), \tag{13}$$

where m_n is the mass of the n-th nucleus, Z_n is the atomic number of the n-th nucleus, p_s is the momentum variable conjugate to s, Q is an effective mass of s that controls the coupling of the system to the heat bath, k_B is the Boltzmann constant, and N_f is the number of degrees of freedom of the system. In this extended system, $p'_{n,j}$ is the conjugate momentum variable to $x_{n,j}$ that is known as a "virtual" momentum variable where the real momentum $p_{n,j}$ can be obtained by $p_{n,j} = \frac{p'_{n,j}}{s}$. The last term E_{el} is the adjustment of the Hamiltonian that adds the ground state electronic energy at a nuclear configuration $\boldsymbol{x}$, which is responsible for the electronic forces. Given this additional degree of freedom s and the use of "virtual momentum", one needs to integrate over the heat bath variable to obtain the actual particle distribution after simulations.

To calculate the ground state electronic energy E_{el}, we require assumptions on the ground state preparation and the separation of ground and excited state energies. For many chemical systems and most biologically relevant systems, where nuclear dynamics is much slower than electronic dynamics, the Born-Oppenheimer approximation can achieve reliable predictions of the system's properties[25,89,90]. Our work primarily operates under this assumption, which precludes the existence of conical intersections between the electronic ground state potential energy surface and the electronic excited state potential energy surface over different nuclear configurations. We further note that the particles in the simulated system in question would be correlated weakly enough such that the Hamiltonians remain sufficiently gapped, leading to a fair assumption that the spectral gap γ is polynomially bounded. Under this assumption, to solve the electronic structure problem at ground state configurations, we assume that we can make use of an approximate ground state oracle U_I that prepares an initial electronic state $|\phi_{\mathrm{init}}(\boldsymbol{x})\rangle$ that has nontrivial overlap with the ground state $|\psi_0(\boldsymbol{x})\rangle$ of the electronic Hamiltonian H_{el} describing the dynamics of the electronic system. Specifically, given $0 < \delta \leq 1$, we demand that for any $\bar{\boldsymbol{x}}$,

$$U_I |\bar{\boldsymbol{x}}\rangle |0\rangle = |\bar{\boldsymbol{x}}\rangle |\phi_{\mathrm{init}}(\boldsymbol{x})\rangle, \tag{14}$$

where $|\langle\psi_0(\boldsymbol{x})|\phi_{\mathrm{init}}(\boldsymbol{x})\rangle| \geq \delta$ for all nuclear configurations. δ is thus a lower bound on the overlap of the prepared approximate state with the true electronic ground state.

While we utilize the initial approximate ground state as generated from a black-box oracle U_I, to implement this in practice, we can borrow methods in classical computational chemistry that provide faster convergence in self-consistent field (SCF) procedures[91] that are nuclear-position independent. These methods include superposition of atomic densities (SAD)[92] and its variants, as well as further refinements with the extended Hückel method[91,93]. Such methods have appeared as wavefunction initialization techniques in computational chemistry packages such as QuantumESPRESSO[94,95] and VASP[96–98], and encode these results into the plane wave basis quantum state to provide an initial guess. Future work on quantizing the implementation of obtaining the Hartree-Fock state, such that it can be prepared in superposition, may further improve ground state preparation.

As in Ref.[29], our quantum algorithm operates within the Liouvillian formalism for simulating Koopman–von Neumann mechanics[99–101]. The Liouvillian formalism allows for the description of the time evolution of a physical system through the Liouville equation of motion:

$$\frac{\partial \rho}{\partial t} = -iL\rho \,, \tag{15}$$

where $\rho(\boldsymbol{x}, \boldsymbol{p}, t)$ can be thought of as the probability density of a system of N classical particles with position $\{\boldsymbol{x}_n\}_{n\in[N]}$ and momentum $\{\boldsymbol{p}_n\}_{n\in[N]}$, and where L is the Liouvillian operator, defined as:

$$L := -i\left(\left(\nabla_{\boldsymbol{p}} H_{\text{ext}}\right) \cdot \nabla_{\boldsymbol{x}} - \left(\nabla_{\boldsymbol{x}} H_{\text{ext}}\right) \cdot \nabla_{\boldsymbol{p}}\right) \,, \tag{16}$$

where H_{ext} is the extended Nosé nuclear Hamiltonian underlying the dynamics of the nuclear system shown above, and is can be separated into the kinetic and potential Hamiltonians H_{kin} and H_{pot} with additional ground state correction terms from the electronic system H_{gse} and extra terms regarding the heat bath H_{bath}. The terms in the sum defining the Liouvillian operator depend directly on the derivatives of the nuclear Hamiltonian H_{ext} with respect to the j-th components of position and momentum of the n-th particle. To map the classical probability density on a quantum computer, we exploit the Koopman-von Neumann description of classical mechanics, which directly connects the probability density to a quantum state[29,102], by defining $\rho := \psi^*_{\text{KvN}}\psi_{\text{KvN}}$. Representing the KvN wavefunction ψ_{KvN} as a quantum state $|\rho\rangle$, the time evolution of the system can be computed as the evolution of the density under the Liouvillian:

$$|\rho_t\rangle = e^{-iLt}\,|\rho_0\rangle \,. \tag{17}$$

This can then be implemented on a quantum computer using Hamiltonian simulation[37,41,42,53,61].

Here, we are interested in MD simulations within the Born-Oppenheimer approximation. The force on the nuclei consists of nuclear and electronic contributions, which we can obtain by considering the two components of the Liouvillian

$$L = L_{\text{cl}} + L_{\text{el}} \,, \tag{18}$$

where the classical part of the Liouvillian L_{cl} is given by the kinetic term and nucleus-nucleus repulsion, and L_{el} adds the quantum interaction between the nuclei and electrons and amongst the electrons, which takes the form of the ground state energy. The electronic Liouvillian can thus be formulated as

$$L_{\text{el}} := i\sum_{n=1}^{N}\sum_{j=1}^{3}\left(\frac{\partial E_{\text{el}}(\boldsymbol{x})}{\partial x_{n,j}}\partial_{p_{n,j}}\right) \,, \tag{19}$$

where E_{el} is the ground state energy. For simulations under the NVT canonical ensemble with the Nosé thermostat, an additional degree of freedom s and its momentum conjugate p_s are additionally considered in the Liouvillian simulation process, but integrated out to retrieve the final probability density $\rho(\boldsymbol{x}, \boldsymbol{p}, t)$. For implementation on a quantum computer, we prepare a set of registers $|\bar{x}_{n,j}\rangle$, $|\bar{p}'_{n,j}\rangle$, $|\bar{s}\rangle$, and $|\bar{p}_s\rangle$ such that operations are only carried out on the relevant registers, where the overbar stands for the discretized phase-space. The "virtual" momentum $\boldsymbol{p'}$ is a reparameterized version of the momentum dependent on both the true momentum $\boldsymbol{p}$ and the heat bath variable s. Details of the spatial discretization and NVT simulation are deferred to Supplementary Information 1.

Prior work by Ref.[29] has shown that a Liouvillian simulation algorithm can be achieved. They show how to efficiently block-encode the classical Liouvillian and implement the evolution with Hamiltonian simulation via quantum singular value transform (QSVT)[37,41,42]. On the other hand, the direct implementation of electronic forces, and by extension, the electronic Liouvillian L_{el}, is circumvented by utilizing controlled Hamiltonian simulation[36], which allows for the implementation $e^{-iL_{\text{el}}t}$ in logarithmic dependency on error. However, since the evolution operator over the electronic Liouvillian L_{el} is implemented directly instead of the full Liouvillian, Trotterization is required to approximate the evolution over the full Liouvillian e^{-iLt}. Their results provide a Liouvillian simulation algorithm with a runtime of

$$\tilde{\mathcal{O}}\left(\frac{N^{2+o(1)}\tilde{N}^{2+o(1)}N_{\text{tot}}^{3+o(1)}t^{1+o(1)}}{\delta\gamma\varepsilon^{o(1)}}\right), \tag{20}$$

where we use $\tilde{\mathcal{O}}(\cdot)$ to hide polylogarithmic factors.

In Supplementary Information 1, we formalize the construction of the electronic Liouvillian L_{el} and further provide technical details required from implementation introduce in prior works, including the formulation and cost of implementing the electronic Hamiltonian H_{el} from Refs.[103,104] and the force operators from Ref.[26] on quantum computers.

B. Alchemical free energy calculation via thermodynamic integration

Thermodynamic quantities such as free energy and entropy can be determined through ensemble averaging over configurations sampled in molecular dynamics or Monte Carlo simulations[11] using appropriate Boltzmann weighting[10]. It is important to distinguish between the Helmholtz free energy, defined at constant volume V as $F = U - TS$, where U is the internal energy and S is entropy, and the Gibbs free energy, defined at constant pressure P as $G = U - TS + PV$[3]. Since experiments are typically carried out at constant pressure, the Gibbs ensemble provides a more realistic representation of physical conditions. Nevertheless, in the context of molecular simulations relevant to drug discovery in aqueous systems, the difference between Gibbs and Helmholtz free energies is negligible, i.e., $\Delta G \approx \Delta F$, because $P\Delta V$ is nearly zero for drug-like molecules in water, as they are effectively incompressible[7,8]. As molecular dynamics often employ constant-volume ensembles, the Helmholtz free energy is often used in computational chemistry. In the following, we will therefore refer to the free energy as F throughout.

We now consider two closely related molecular systems, A and B, with a large phase space overlap and with microstate energies $E_{\mathcal{S}}(A)$ and $E_{\mathcal{S}}(B)$ where $\mathcal{S}$ labels the microstates, corresponding to different molecular geometries, in the NVT canonical ensemble. These molecular systems differ by only one atom or functional group, resulting in significant overlap in nuclear phase-space. Computing the absolute free energy of both systems requires extensive sampling for reliable convergence, making the process computationally demanding. As an alternative, we can employ a method that focuses solely on calculating the free energy difference ΔF of systems A and B, which reduces the required sampling and computational cost[2–5,9].

Consider a new system with microstate energy functions $E_{\mathcal{S}}(\Lambda)$ which are differentiable functions of a new coupling parameter $\Lambda \in [0, 1]$ satisfying

$$E_{\mathcal{S}}(0) = E_{\mathcal{S}}(A) \tag{21}$$

$$E_{\mathcal{S}}(1) = E_{\mathcal{S}}(B)\,. \tag{22}$$

To obtain the free energy in an NVT canonical ensemble, we need to consider the partition function of the system:

$$Z(N, V, T, \Lambda) = \sum_{\mathcal{S}} \exp(-E_{\mathcal{S}}(\Lambda)/k_B T)\,. \tag{23}$$

The microstates $\mathcal{S}$ accessible to the system depend on the number of particles N, the volume V, and the temperature T. A sufficient number of states $\mathcal{S}$ must be chosen so that the partition function converges. Under Liouvillian simulation in the NVT canonical ensemble, we can directly obtain a phase-space density over such states. The Helmholtz free energy of this system is given by

$$F(N, V, T, \Lambda) = -k_B T \ln Z(N, V, T, \Lambda)\,. \tag{24}$$

Helmholtz free energy differences are important because they approximate Gibbs free energy differences in aqueous solutions.

However, when solely calculating the free energy difference ΔF, the explicit calculation of the partition function can be avoided. The integral over the derivative of the free energy gives the free energy difference from A to B,

$$\begin{aligned}\Delta F_{A\to B} &= \int_0^1 \frac{\partial F(\Lambda)}{\partial \Lambda} d\Lambda \\ &= -k_B T \int_0^1 \frac{1}{Z}\frac{\partial Z}{\partial \Lambda} d\Lambda \\ &= \int_0^1 \frac{1}{Z}\sum_{\mathcal{S}} \frac{\partial E_{\mathcal{S}}(\Lambda)}{\partial \Lambda} e^{-E_{\mathcal{S}}(\Lambda)/k_B T} d\Lambda \\ &= \int_0^1 \left\langle \frac{\partial E(\Lambda)}{\partial \Lambda} \right\rangle_\Lambda d\Lambda\,, \end{aligned} \tag{25}$$

where the angular brackets denote an ensemble-averaged derivative of the microstate energies with respect to the coupling parameter Λ over the thermal distribution of the states $\mathcal{S}$ for a particular coupling parameter Λ. As noted, the distribution is provided by equilibration via the NVT canonical ensemble, so the partition function need not be further computed. Thus, under this scheme, rather than computing the derivative of the free energy directly, only the expectation value of the derivative of the microstate energy needs to be evaluated[3].

When choosing $E_{\mathcal{S}}(\Lambda)$ as a linear function between the microstate energies of system A and system B,

$$E_{\mathcal{S}}(\Lambda) = E_{\mathcal{S}}(A) + \Lambda(E_{\mathcal{S}}(B) - E_{\mathcal{S}}(A)), \tag{26}$$

we obtain

$$\Delta F_{A\to B} = \int_0^1 \langle E(B) - E(A)\rangle_\Lambda \, d\Lambda. \tag{27}$$

In practice, the integral is discretized by calculating the expectation values for a discrete number of values of Λ. Then, to determine the difference in free energy from A to B, the expectation values are summed over all values of Λ, yielding the following approximate free energy difference:

$$\Delta\tilde{F} := \frac{1}{N_\Lambda}\sum_{\Lambda} \langle E(B) - E(A)\rangle_\Lambda\,. \tag{28}$$

Note that while we choose a linear path here for simplicity, selecting a non-linear path may be advantageous because the instantaneous difference in the block encoding constants for nuclear Hamiltonians H_A and H_B that are used to compute the internal energies $\langle E_A\rangle$ and $\langle E_B\rangle$ may be chosen to be far smaller for such a thermodynamic integration rather than the differences, which can lead to smaller costs for the overall calculation as discussed in Ref.[105].

Under the Liouvillian formalism, the thermal distribution is obtained by evolving the phase-space density with the NVT canonical Liouvillian for some sufficient equilibration time t_{eq}, while thermal averages are obtained by taking the expectation value of the relevant operator over the thermal distribution for each point in the phase-space. In our case, where a quantum state on registers represents the thermal distribution, the computational basis corresponds to a point in the discretized phase-space, and the square of the corresponding amplitude would be its probability. The microstate energies over the phase-space can then be encoded into a diagonal matrix to form the nuclear Hamiltonian, with each entry corresponding to the microstate energy at the relevant point in phase-space.

C. Block encodings and quantum linear algebra

We assume access to operators such as Hamiltonians and forces in the form of block encodings[36,37] in this paper.

A block encoding is an encoding scheme that embeds a general matrix into the top left corner of a unitary matrix, such that

$$|A - \alpha(\langle 0^a| \otimes \mathbb{I}_n)U_A(|0^a\rangle \otimes \mathbb{I}_n)| \leq \varepsilon\,. \tag{29}$$

This embedding of A into a unitary U_A is then known as a (α, a, ε)-block-encoding of A. In the main text, we refer to α as the scaling factor of the block encoding when mentioned in isolation.

To manipulate such block encodings, we can use a framework known as quantum singular value transformation (QSVT)[37], which can be used to apply a polynomial transformation to the singular values of the matrix A such that

$$\mathrm{QSVT}(U_A) = \begin{bmatrix} \mathrm{Poly}^{(\mathrm{SV})}(A) & * \\ * & * \end{bmatrix}. \tag{30}$$

In the case of Hermitian matrices, the transformations are applied to the eigenvalues of the matrix. We refer the reader to Supplementary Information 2 for a detailed account of QSVT as a quantum linear algebra toolbox to perform ground state preparation[48] and Hamiltonian simulation[37,41,42], which are subroutines used in our main results. The reader will also find a brief review on quantum signal processing (QSP) without angle finding[55]. Furthermore, we deferred several new results to the Supplementary Information that were derived as part of our proofs, such as algorithms for robust ground state preparation and robust Hamiltonian simulation via QSP without angle finding.

DATA AVAILABILITY

This manuscript does not report data generation or analysis.

CODE AVAILABILITY

This manuscript does not report any new code. All algorithmic details necessary for implementation are described explicitly in the manuscript.

ACKNOWLEDGMENTS

PWH, GB, DMD, HJ, TRB, and BK thank Zhu Sun, Zhenyu Cai, and Simon Benjamin for valuable discussions and their support during the project, as well as Annina Lieberherr for her comments on the manuscript and discussions on MD simulations. PWH would also like to thank Wei-Tse Hsu for discussions on classical MD simulations and rare events, as well as Jon Keating and Sakura Schafer-Nameki for comments on the initial preprint manuscript. GLRA, MD, NM, RS, MS, and BR thank Clemens Utschig-Utschig for his comments on the manuscript and his support during the project.

FUNDING

PWH acknowledges support from the Engineering and Physical Sciences Research Council (EPSRC) Doctoral Training Partnership (EP/W524311/1) with a CASE Conversion Studentship in collaboration with Quantum Motion. DMD acknowledges financial support from the EPSRC Hub in Quantum Computing and Simulation (EP/T001062/1). NW and SS's work was supported by support from Boehringer Ingelheim and the U.S. Department of Energy, Office of Science, National Quantum Information Science Research Centers, Co-design Center for Quantum Advantage (C2QA) under contract number DE-SC0012704 (PNNL FWP 76274). NW's research is also supported by PNNL's Quantum Algorithms and Architecture for Domain Science (QuAADS) Laboratory Directed Research and Development (LDRD) Initiative. The Pacific Northwest National Laboratory is operated by Battelle for the U.S. Department of Energy under Contract DE-AC05-76RL01830. BK thanks UKRI for the Future Leaders Fellowship Theory to Enable Practical Quantum Advantage (MR/Y015843/1). BK also acknowledges funding from the EPSRC projects Robust and Reliable Quantum Computing (RoaRQ, EP/W032635/1) and Software Enabling Early Quantum Advantage (SEEQA, EP/Y004655/1).

COMPETING INTERESTS

Bálint Koczor is an Associate Editor of npj Quantum Information. Bálint Koczor was not involved in the journal's review of, or decisions related to, this manuscript.

AUTHOR CONTRIBUTIONS

PWH provided the main quantum algorithmic subroutines, completed proofs, and drafted the result sections and the supplementary material. GB proposed the use of angleless QSP and algorithmic methods for alchemical calculations and wrote the initial draft for relevant sections. BK proposed the use of the Hellmann-Feynman theorem. NM and BR proposed the use of thermodynamic integration. NM, RS, and DMD drafted the introduction. PWH, DMD, and NW drafted the discussion. PWH, GB, MD, NM, RS, MS, and SS drafted the preliminaries. HJ checked the correctness of all proofs and algorithms. GLRA, MD, NM, RS, MS, NW, TRB, and BK conceived of the project. All authors contributed to the conceptualization and discussion behind the main research ideas, as well as reviewing and editing the manuscript.

REFERENCES

[1] Chodera, J. D. *et al.* Alchemical free energy methods for drug discovery: progress and challenges. *Curr. Opin.*

Struct. Biol. **21**, 150–160 (2011). URL https://doi.org/10.1016/j.sbi.2011.01.011.

[2] de Ruiter, A., Petrov, D. & Oostenbrink, C. Optimization of alchemical pathways using extended thermodynamic integration. *J. Chem. Theory Comput.* **17**, 56–65 (2021). URL https://doi.org/10.1021/acs.jctc.0c01170.

[3] Frenkel, D. & Smit, B. *Understanding Molecular Simulation: From Algorithms to Applications* (Academic Press, Inc., USA, 1996). URL https://doi.org/10.1016/C2009-0-63921-0.

[4] Kästner, J., Senn, H. M., Thiel, S., Otte, N. & Thiel, W. QM/MM free-energy perturbation compared to thermodynamic integration and umbrella sampling: Application to an enzymatic reaction. *J. Chem. Theory Comput.* **2**, 452–461 (2006). URL https://doi.org/10.1021/ct050252w.

[5] Cournia, Z., Allen, B. & Sherman, W. Relative binding free energy calculations in drug discovery: Recent advances and practical considerations. *J. Chem. Inf. Model.* **57**, 2911–2937 (2017). URL https://doi.org/10.1021/acs.jcim.7b00564.

[6] Shirts, M. R., Mobley, D. L. & Chodera, J. D. *Chapter 4 Alchemical Free Energy Calculations: Ready for Prime Time?*, vol. 3, 41–59 (Elsevier, 2007). URL https://doi.org/10.1016/S1574-1400(07)03004-6.

[7] Mey, A. S. *et al.* Best practices for alchemical free energy calculations. *Living J. Comp. Mol. Sci.* **2** (2020). URL https://doi.org/10.33011/livecoms.2.1.18378.

[8] de Jong, D. H. *et al.* Determining equilibrium constants for dimerization reactions from molecular dynamics simulations. *J. Comput. Chem* **32**, 1919–1928 (2011). URL https://doi.org/10.1002/jcc.21776.

[9] Kirkwood, J. G. Statistical mechanics of fluid mixtures. *J. Chem. Phys.* **3**, 300–313 (1935). URL https://doi.org/10.1063/1.1749657.

[10] Zwanzig, R. W. High-temperature equation of state by a perturbation method. II. Polar gases. *J. Chem. Phys.* **23**, 1915–1922 (1955). URL https://doi.org/10.1063/1.1740604.

[11] Bennett, C. H. Efficient estimation of free energy differences from Monte Carlo data. *J. Comput. Phys.* **22**, 245–268 (1976). URL https://doi.org/10.1016/0021-9991(76)90078-4.

[12] Allen, M. P. & Tildesley, D. J. *Computer Simulation of Liquids* (Oxford University Press, 1987). URL https://doi.org/10.1093/oso/9780198803195.001.0001.

[13] Williams-Noonan, B. J., Yuriev, E. & Chalmers, D. K. Free energy methods in drug design: Prospects of "alchemical perturbation" in medicinal chemistry. *J. Med. Chem.* **61**, 638–649 (2018). URL https://doi.org/10.1021/acs.jmedchem.7b00681.

[14] Hansen, N. & van Gunsteren, W. F. Practical aspects of free-energy calculations: A review. *J. Chem. Theory Comput.* **10**, 2632–2647 (2014). URL https://doi.org/10.1021/ct500161f.

[15] Feynman, R. P. Simulating physics with computers. *Int. J. Theor. Phys.* **21**, 467–488 (1982). URL https://doi.org/10.1007/BF02650179.

[16] Lloyd, S. Universal quantum simulators. *Science* **273**, 1073–1078 (1996). URL https://doi.org/10.1126/science.273.5278.1073.

[17] Caesura, A. *et al.* Faster quantum chemistry simulations on a quantum computer with improved tensor factorization and active volume compilation. *PRX Quantum* **6**, 030337 (2025). URL https://doi.org/10.1103/yngp-5fpm.

[18] Low, G. H. *et al.* Fast quantum simulation of electronic structure by spectral amplification. *Phys. Rev. X* **15**, 041016 (2025). URL https://doi.org/10.1103/pb2g-j9cw.

[19] Reiher, M., Wiebe, N., Svore, K. M., Wecker, D. & Troyer, M. Elucidating reaction mechanisms on quantum computers. *Proc. Natl. Acad. Sci. U.S.A.* **114**, 7555–7560 (2017). URL https://doi.org/10.1073/pnas.1619152114.

[20] McArdle, S., Endo, S., Aspuru-Guzik, A., Benjamin, S. C. & Yuan, X. Quantum computational chemistry. *Rev. Mod. Phys.* **92**, 015003 (2020). URL https://doi.org/10.1103/RevModPhys.92.015003.

[21] von Burg, V. *et al.* Quantum computing enhanced computational catalysis. *Phys. Rev. Res.* **3**, 033055 (2021). URL https://doi.org/10.1103/PhysRevResearch.3.033055.

[22] Outeiral, C. *et al.* The prospects of quantum computing in computational molecular biology. *Wiley Interdiscip. Rev. Comput. Mol. Sci.* **11**, e1481 (2021). URL https://doi.org/10.1002/wcms.1481.

[23] Rubin, N. C. *et al.* Fault-tolerant quantum simulation of materials using Bloch orbitals. *PRX Quantum* **4**, 040303 (2023). URL https://doi.org/10.1103/PRXQuantum.4.040303.

[24] Santagati, R. *et al.* Drug design on quantum computers. *Nat. Phys.* **20**, 549–557 (2024). URL https://doi.org/10.1038/s41567-024-02411-5.

[25] Born, M. & Oppenheimer, R. Zur Quantentheorie der Molekeln. *Ann. Phys. (Leipzig)* **389**, 457–484 (1927). URL https://onlinelibrary.wiley.com/doi/abs/10.1002/andp.19273892002.

[26] O'Brien, T. E. *et al.* Efficient quantum computation of molecular forces and other energy gradients. *Phys. Rev. Res.* **4**, 043210 (2022). URL https://doi.org/10.1103/PhysRevResearch.4.043210.

[27] Steudtner, M. *et al.* Fault-tolerant quantum computation of molecular observables. *Quantum* **7**, 1164 (2023). URL https://doi.org/10.22331/q-2023-11-06-1164.

[28] Günther, J. *et al.* How to use quantum computers for biomolecular free energies (2025). URL https://doi.org/10.48550/arXiv.2506.20587. 2506.20587.

[29] Simon, S. *et al.* Improved precision scaling for simulating coupled quantum-classical dynamics. *PRX Quantum* **5**, 010343 (2024). URL https://doi.org/10.1103/PRXQuantum.5.010343.

[30] Gonzalez-Conde, J. & Sornborger, A. T. Mixed quantum-semiclassical simulation (2023). URL https://doi.org/10.48550/arXiv.2308.16147. 2308.16147.

[31] Liouville, J. Sur la théorie de la variation des constantes arbitraires. *J. Math. Pures Appl.* 342–349 (1838). URL https://eudml.org/doc/234417.

[32] Cleve, R., Ekert, A., Macchiavello, C. & Mosca, M. Quantum algorithms revisited. *Proc. R. Soc. Lond., A: Math. Phys. Eng. Sci.* **454**, 339–354 (1998). URL https://doi.org/10.1098/rspa.1998.0164.

[33] Suzuki, M. Generalized Trotter's formula and systematic approximants of exponential operators and inner derivations with applications to many-body problems. *Commun. Math. Phys.* **51**, 183–190 (1976). URL https://doi.org/10.1007/BF01609348.

[34] Childs, A. M., Su, Y., Tran, M. C., Wiebe, N. & Zhu, S. Theory of Trotter error with commutator scaling. *Phys. Rev. X* **11**, 011020 (2021). URL `https://doi.org/10.1103/PhysRevX.11.011020`.

[35] Berry, D. W., Childs, A. M., Cleve, R., Kothari, R. & Somma, R. D. Simulating Hamiltonian dynamics with a truncated Taylor series. *Phys. Rev. Lett.* **114**, 090502 (2015). URL `https://doi.org/10.1103/PhysRevLett.114.090502`.

[36] Chakraborty, S., Gilyén, A. & Jeffery, S. The power of block-encoded matrix powers: Improved regression techniques via faster Hamiltonian simulation. In Baier, C., Chatzigiannakis, I., Flocchini, P. & Leonardi, S. (eds.) *46th International Colloquium on Automata, Languages, and Programming (ICALP 2019)*, vol. 132 of *Leibniz International Proceedings in Informatics (LIPIcs)*, 33:1–33:14 (Schloss Dagstuhl – Leibniz-Zentrum für Informatik, 2019). URL `https://doi.org/10.4230/LIPIcs.ICALP.2019.33`.

[37] Gilyén, A., Su, Y., Low, G. H. & Wiebe, N. Quantum singular value transformation and beyond: Exponential improvements for quantum matrix arithmetics. In *Proceedings of the 51st Annual ACM SIGACT Symposium on Theory of Computing*, STOC 2019, 193–204 (Association for Computing Machinery, New York, NY, USA, 2019). URL `https://doi.org/10.1145/3313276.3316366`.

[38] Low, G. H. & Wiebe, N. Hamiltonian simulation in the interaction picture (2018). URL `https://doi.org/10.48550/arXiv.1805.00675`. 1805.00675.

[39] Trotter, H. F. On the product of semi-groups of operators. *Proc. Am. Math. Soc.* **10**, 545–551 (1959). URL `https://doi.org/10.1090/S0002-9939-1959-0108732-6`.

[40] Suzuki, M. General theory of fractal path integrals with applications to many-body theories and statistical physics. *J. Math. Phys.* **32**, 400–407 (1991). URL `https://doi.org/10.1063/1.529425`.

[41] Low, G. H. & Chuang, I. L. Optimal Hamiltonian simulation by quantum signal processing. *Phys. Rev. Lett.* **118**, 010501 (2017). URL `https://doi.org/10.1103/PhysRevLett.118.010501`.

[42] Low, G. H. & Chuang, I. L. Hamiltonian simulation by qubitization. *Quantum* **3**, 163 (2019). URL `https://doi.org/10.22331/q-2019-07-12-163`.

[43] Gilyén, A. & Li, T. Distributional property testing in a quantum world. In Vidick, T. (ed.) *11th Innovations in Theoretical Computer Science Conference (ITCS 2020)*, vol. 151 of *Leibniz International Proceedings in Informatics (LIPIcs)*, 25:1–25:19 (Schloss Dagstuhl – Leibniz-Zentrum für Informatik, Dagstuhl, Germany, 2020). URL `https://doi.org/10.4230/LIPIcs.ITCS.2020.25`.

[44] Brassard, G., Høyer, P., Mosca, M. & Tapp, A. Quantum amplitude amplification and estimation. In *Quantum computation and information*, vol. 305 of *Contemporary Mathematics*, 53–74 (American Mathematical Society, Providence, RI, USA, 2002). URL `https://doi.org/10.1090/conm/305/05215`.

[45] Hellmann, H. *Einführung in die Quantenchemie* (Franz Deuticke, Leipzig, 1937). URL `https://doi.org/10.1007/978-3-662-45967-6`.

[46] Feynman, R. P. Forces in molecules. *Phys. Rev.* **56**, 340–343 (1939). URL `https://doi.org/10.1103/PhysRev.56.340`.

[47] Kitaev, A. Y. Quantum measurements and the abelian stabilizer problem (1995). URL `https://doi.org/10.48550/arXiv.quant-ph/9511026`. quant-ph/9511026.

[48] Lin, L. & Tong, Y. Near-optimal ground state preparation. *Quantum* **4**, 372 (2020). URL `https://doi.org/10.22331/q-2020-12-14-372`.

[49] Szegedy, M. Quantum speed-up of Markov chain based algorithms. In *45th Annual IEEE Symposium on Foundations of Computer Science*, 32–41 (2004). URL `https://doi.org/10.1109/FOCS.2004.53`.

[50] Knill, E., Ortiz, G. & Somma, R. D. Optimal quantum measurements of expectation values of observables. *Phys. Rev. A* **75**, 012328 (2007). URL `https://doi.org/10.1103/PhysRevA.75.012328`.

[51] Pulay, P. Ab initio calculation of force constants and equilibrium geometries in polyatomic molecules: I. theory. *Mol. Phys.* **17**, 197–204 (1969). URL `https://doi.org/10.1080/00268976900100941`.

[52] Francis, G. P. & Payne, M. C. Finite basis set corrections to total energy pseudopotential calculations. *J. Phys.: Condens. Matter* **2**, 4395–4404 (1990). URL `https://doi.org/10.1088/0953-8984/2/19/007`.

[53] Childs, A. M. & Wiebe, N. Hamiltonian simulation using linear combinations of unitary operations. *Quantum Info. Comput.* **12**, 901–924 (2012). URL `https://doi.org/10.26421/QIC12.11-12-1`.

[54] Istrail, S. Statistical mechanics, three-dimensionality and NP-completeness: I. Universality of intracatability for the partition function of the Ising model across non-planar surfaces (extended abstract). In *Proceedings of the Thirty-Second Annual ACM Symposium on Theory of Computing*, STOC '00 (Association for Computing Machinery, New York, NY, USA, 2000). URL `https://doi.org/10.1145/335305.335316`.

[55] Alase, A. Quantum signal processing without angle finding (2025). URL `https://doi.org/10.48550/arXiv.2501.07002`. 2501.07002.

[56] Chao, R., Ding, D., Gilyen, A., Huang, C. & Szegedy, M. Finding angles for quantum signal processing with machine precision (2020). URL `https://doi.org/10.48550/arXiv.2003.02831`. 2003.02831.

[57] Dong, Y., Meng, X., Whaley, K. B. & Lin, L. Efficient phase-factor evaluation in quantum signal processing. *Phys. Rev. A* **103** (2021). URL `https://doi.org/10.1103/PhysRevA.103.042419`.

[58] Wang, J., Dong, Y. & Lin, L. On the energy landscape of symmetric quantum signal processing. *Quantum* **6**, 850 (2022). URL `https://doi.org/10.22331/q-2022-11-03-850`.

[59] Motlagh, D. & Wiebe, N. Generalized quantum signal processing. *PRX Quantum* **5**, 020368 (2024). URL `https://doi.org/10.1103/PRXQuantum.5.020368`.

[60] Vedral, V., Barenco, A. & Ekert, A. Quantum networks for elementary arithmetic operations. *Phys. Rev. A* **54**, 147–153 (1996). URL `https://doi.org/10.1103/PhysRevA.54.147`.

[61] Berry, D. W., Childs, A. M., Cleve, R., Kothari, R. & Somma, R. D. Exponential improvement in precision for simulating sparse Hamiltonians. In *Proceedings of the Forty-Sixth Annual ACM Symposium on Theory of Computing*, STOC '14, 283–292 (Association for Computing Machinery, New York, NY, USA, 2014). URL `https://doi.org/10.1145/2591796.2591854`.

[62] Jorge, M., Garrido, N. M., Queimada, A. J., Economou, I. G. & Macedo, E. A. Effect of the integration method on the accuracy and computational efficiency of free

energy calculations using thermodynamic integration. *J. Chem. Theory Comput.* **6**, 1018–1027 (2010). URL https://doi.org/10.1021/ct900661c.

[63] Metropolis, N. & Ulam, S. The Monte Carlo method. *J. Am. Stat. Assoc.* **44**, 335–341 (1949). URL https://doi.org/10.1080/01621459.1949.10483310.

[64] Montanaro, A. Quantum speedup of Monte Carlo methods. *Proc. R. Soc. A: Math. Phys. Eng. Sci.* **471**, 20150301 (2015). URL https://doi.org/10.1098/rspa.2015.0301.

[65] Szabó, A. & Ostlund, N. S. *Modern Quantum Chemistry: Introduction to Advanced Electronic Structure Theory* (Dover Publications, 1996). URL https://store.doverpublications.com/products/9780486691862.

[66] Breuckmann, N. P. & Terhal, B. M. Space-time circuit-to-Hamiltonian construction and its applications. *J. Phys. A: Math. Theor.* **47**, 195304 (2014). URL https://doi.org/10.1088/1751-8113/47/19/195304.

[67] Verlet, L. Computer "experiments" on classical fluids. I. Thermodynamical properties of Lennard-Jones molecules. *Phys. Rev.* **159**, 98–103 (1967). URL https://doi.org/10.1103/PhysRev.159.98.

[68] Tuckerman, M., Berne, B. J. & Martyna, G. J. Reversible multiple time scale molecular dynamics. *J. Chem. Phys.* **97**, 1990–2001 (1992). URL https://doi.org/10.1063/1.463137.

[69] Yoshida, H. Construction of higher order symplectic integrators. *Phys. Lett. A* **150**, 262–268 (1990). URL https://doi.org/10.1016/0375-9601(90)90092-3.

[70] Cancés, E. *et al.* Long-time averaging for integrable hamiltonian dynamics. *Num. Math.* **100**, 211–232 (2005). URL https://doi.org/10.1007/s00211-005-0599-0.

[71] Cancès, E. *et al.* High-order averaging schemes with error bounds for thermodynamical properties calculations by molecular dynamics simulations. *J. Chem. Phys.* **121**, 10346–10355 (2004). URL https://doi.org/10.1063/1.1794611.

[72] Deutsch, J. M. Eigenstate thermalization hypothesis. *Rep. Prog. Phys.* **81**, 082001 (2018). URL https://doi.org/10.1088/1361-6633/aac9f1.

[73] Shirai, T. & Mori, T. Thermalization in open many-body systems based on eigenstate thermalization hypothesis. *Phys. Rev. E* **101**, 042116 (2020). URL https://doi.org/10.1103/PhysRevE.101.042116.

[74] Chen, C.-F. & Brandão, F. G. S. L. Fast thermalization from the eigenstate thermalization hypothesis (2023). URL https://doi.org/10.48550/arXiv.2112.07646. 2112.07646.

[75] Almeida, G., Ribeiro, P., Haque, M. & Sá, L. Universality, robustness, and limits of the eigenstate thermalization hypothesis in open quantum systems (2025). URL https://doi.org/10.48550/arXiv.2504.10261. 2504.10261.

[76] Bennett, C. H. *Molecular Dynamics and Transition State Theory: The Simulation of Infrequent Events*, 63–97 (American Chemical Society, 1977). URL https://doi.org/10.1021/bk-1977-0046.ch004.

[77] Chandler, D. Statistical mechanics of isomerization dynamics in liquids and the transition state approximation. *J. Chem. Phys.* **68**, 2959–2970 (1978). URL https://doi.org/10.1063/1.436049.

[78] Chen, C.-F., Kastoryano, M. J., Brandão, F. G. S. L. & Gilyén, A. Quantum thermal state preparation (2023). URL https://doi.org/10.48550/arXiv.2303.18224. 2303.18224.

[79] Rall, P., Wang, C. & Wocjan, P. Thermal state preparation via rounding promises. *Quantum* **7**, 1132 (2023). URL https://doi.org/10.22331/q-2023-10-10-1132.

[80] Ramkumar, A. & Soleimanifar, M. Mixing Time of Quantum Gibbs Sampling for Random Sparse Hamiltonians. In Fefferman, B. (ed.) *20th Conference on the Theory of Quantum Computation, Communication and Cryptography (TQC 2025)*, vol. 350 of *Leibniz International Proceedings in Informatics (LIPIcs)*, 3:1–3:23 (Schloss Dagstuhl – Leibniz-Zentrum für Informatik, Dagstuhl, Germany, 2025). URL https://doi.org/10.4230/LIPIcs.TQC.2025.3.

[81] Rouzé, C., França, D. S. & Alhambra, Á. M. Optimal quantum algorithm for Gibbs state preparation (2024). URL https://doi.org/10.48550/arXiv.2411.04885. 2411.04885.

[82] Tong, Y. & Zhan, Y. Fast mixing of weakly interacting fermionic systems at any temperature. *PRX Quantum* **6**, 030301 (2025). URL https://doi.org/10.1103/h1dx-ps5p.

[83] Šmíd, Š., Meister, R., Berta, M. & Bondesan, R. Polynomial-time quantum gibbs sampling for the weak and strong coupling regime of the fermi-hubbard model at any temperature. *Nat. Commun.* **16** (2025). URL https://doi.org/10.1038/s41467-025-65765-1.

[84] Metropolis, N., Rosenbluth, A. W., Rosenbluth, M. N., Teller, A. H. & Teller, E. Equation of state calculations by fast computing machines. *J. Chem. Phys.* **21**, 1087–1092 (1953). URL https://doi.org/10.1063/1.1699114.

[85] Hastings, W. K. Monte Carlo sampling methods using Markov chains and their applications. *Biometrika* **57**, 97–109 (1970). URL https://doi.org/10.1093/biomet/57.1.97.

[86] Gibbs, J. W. *Elementary Principles in Statistical Mechanics: Developed with Especial Reference to the Rational Foundation of Thermodynamics* (Cambridge University Press, 1902). URL https://doi.org/10.1017/CBO9780511686948.

[87] Nosé, S. A molecular dynamics method for simulations in the canonical ensemble. *Mole. Phys.* **52**, 255–268 (1984). URL https://doi.org/10.1080/00268978400101201.

[88] Nosé, S. A unified formulation of the constant temperature molecular dynamics methods. *J. Chem. Phys.* **81**, 511–519 (1984). URL https://doi.org/10.1063/1.447334.

[89] Tully, J. C. Perspective on "Zur Quantentheorie der Molekeln". *Theor. Chem. Acc.* **103**, 173–176 (2000). URL https://doi.org/10.1007/s002149900049.

[90] Bransden, B. & Joachain, C. *Physics of atoms and molecules* (Pearson Education, 2003), 2nd edn. URL https://www.google.com/books/edition/_/bAYV5sgcXrwC.

[91] Lehtola, S. Assessment of initial guesses for self-consistent field calculations. superposition of atomic potentials: Simple yet efficient. *J. Chem. Theory Comput.* **15**, 1593–1604 (2019). URL https://doi.org/10.1021/acs.jctc.8b01089.

[92] Van Lenthe, J. H., Zwaans, R., Van Dam, H. J. J. & Guest, M. F. Starting SCF calculations by superposition of atomic densities. *Journal of Computational Chemistry* **27**, 926–932 (2006). URL https://doi.org/10.1002/

jcc.20393.

[93] Hoffmann, R. An extended Hückel theory. I. hydrocarbons. *J. Chem. Phys.* **39**, 1397–1412 (1963). URL https://doi.org/10.1063/1.1734456.

[94] Giannozzi, P. *et al.* Quantum ESPRESSO: a modular and open-source software project for quantum simulations of materials. *J. Phys.: Condens. Matter* **21**, 395502 (2009). URL https://doi.org/10.1088/0953-8984/21/39/395502.

[95] Giannozzi, P. *et al.* Advanced capabilities for materials modelling with quantum ESPRESSO. *J. Phys.: Condens. Matter* **29**, 465901 (2017). URL https://doi.org/10.1088/1361-648X/aa8f79.

[96] Kresse, G. & Hafner, J. Ab initio molecular dynamics for liquid metals. *Phys. Rev. B* **47**, 558–561 (1993). URL https://doi.org/10.1103/PhysRevB.47.558.

[97] Kresse, G. & Furthmüller, J. Efficiency of ab-initio total energy calculations for metals and semiconductors using a plane-wave basis set. *Comput. Mater. Sci.* **6**, 15–50 (1996). URL https://doi.org/10.1016/0927-0256(96)00008-0.

[98] Kresse, G. & Furthmüller, J. Efficient iterative schemes for ab initio total-energy calculations using a plane-wave basis set. *Phys. Rev. B* **54**, 11169–11186 (1996). URL https://doi.org/10.1103/PhysRevB.54.11169.

[99] Koopman, B. O. Hamiltonian systems and transformation in Hilbert space. *Proc. Natl. Acad. Sci. U.S.A.* **17**, 315–318 (1931). URL https://doi.org/10.1073/pnas.17.5.315.

[100] von Neumann, J. Zur Operatorenmethode in der Klassischen Mechanik. *Ann. Math.* **33**, 587 (1932). URL https://doi.org/10.2307/1968537.

[101] von Neumann, J. Zusatze zur Arbeit "Zur Operatorenmethode"... *Ann. Math.* **33**, 789 (1932). URL https://doi.org/10.2307/1968225.

[102] Mauro, D. On Koopman–von Neumann waves. *Int. J. Mod. Phys. A* **17**, 1301–1325 (2002). URL https://doi.org/10.1142/S0217751X02009680.

[103] Babbush, R., Berry, D. W., McClean, J. R. & Neven, H. Quantum simulation of chemistry with sublinear scaling in basis size. *npj Quantum Inf.* **5** (2019). URL https://doi.org/10.1038/s41534-019-0199-y.

[104] Su, Y., Berry, D. W., Wiebe, N., Rubin, N. & Babbush, R. Fault-tolerant quantum simulations of chemistry in first quantization. *PRX Quantum* **2**, 040332 (2021). URL https://doi.org/10.1103/PRXQuantum.2.040332.

[105] Simon, S. *et al.* Amplified amplitude estimation: Exploiting prior knowledge to improve estimates of expectation values (2024). URL https://doi.org/10.48550/arXiv.2402.14791. 2402.14791.

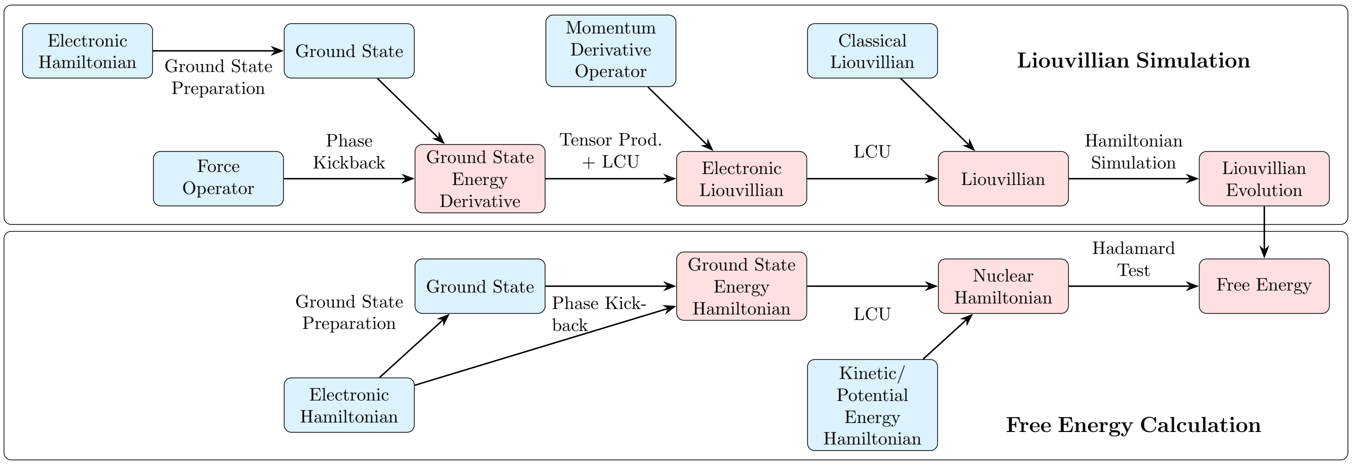

FIGURE 1. *Overview of our algorithm construction.* The results in the top panel of the figure regarding the efficient construction of a Liouvillian simulation quantum algorithm are featured in Section II A. In addition, the results in the bottom panel of the figure for the design of a quantum algorithm for alchemical free energy calculation are featured in Section II B. In this figure, we color our technical contributions in red, while those from existing work are colored in cyan. For the Liouvillian simulation algorithm, we use the Hellmann-Feynman theorem[45,46] to efficiently construct a diagonal block encoding of the ground state energy derivative for each point in phase-space, which is then used to construct the electronic and full Liouvillians. Subsequently, using Hamiltonian simulation[37,41,42], we can implement a Liouvillian evolution operator with logarithmic dependency on precision. Integrating these results with an efficient block encoding of the nuclear Hamiltonian, we can find the free energy difference between two systems through implementing the thermodynamic integration[3] via the Hadamard test[32,47].

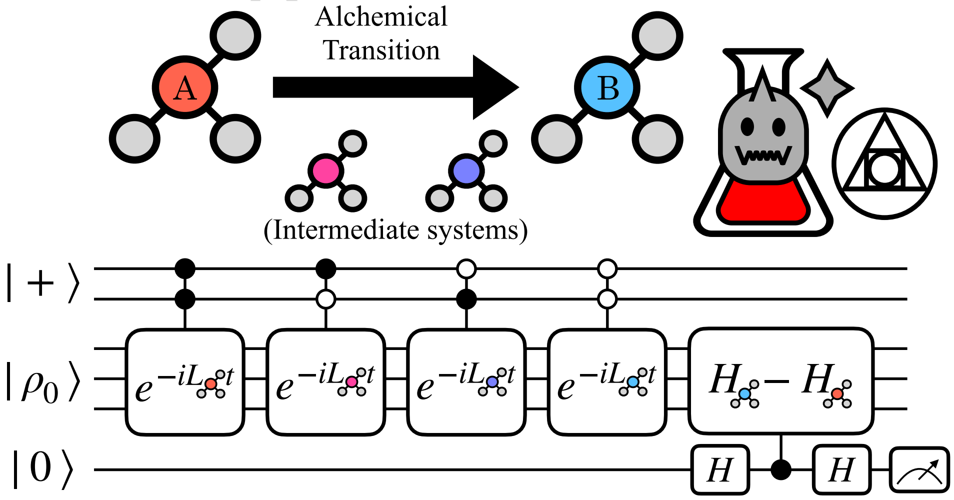

FIGURE 2. *Alchemic free energy calculation on a quantum computer.* Given systems A and B, we perform Liouvillian simulations of the two systems and their interpolated intermediate systems in superposition. Note that while the operators are shown separately in this illustration, we implement them as one single operator via controlled weighting of LCU components without the multiplicative cost of executing separate simulations for each intermediate system. We then compute the internal energy difference and sum over the different results via the Hadamard test to provide the free energy difference.

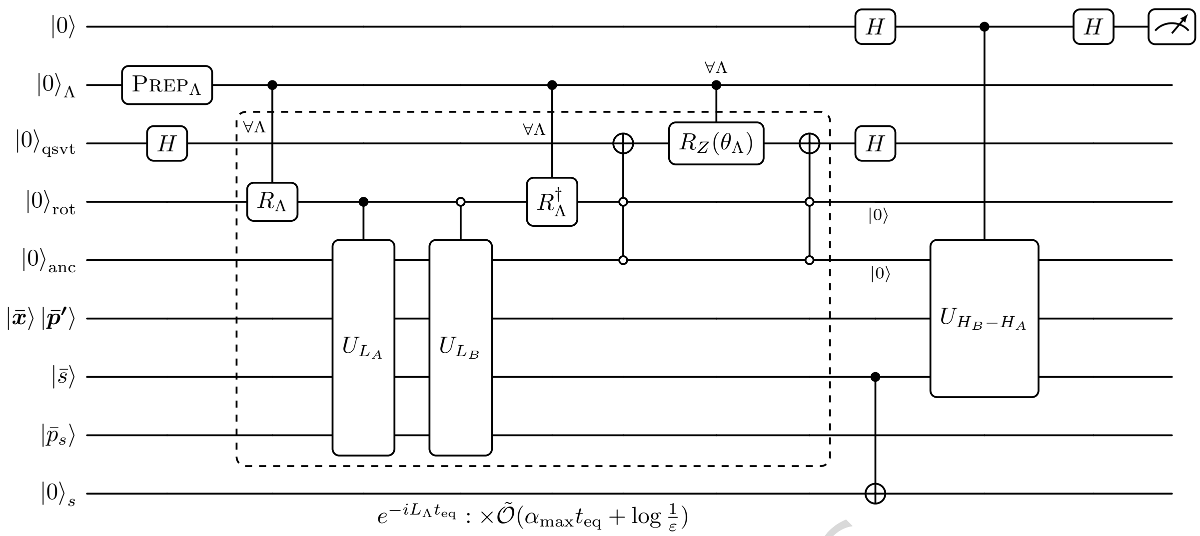

FIGURE 3. *Circuit for obtaining the free energy difference.* The dashed block indicates the repeated linear combination of block encodings to produce a block encoding of L_Λ, which is then transformed to $e^{-iL_\Lambda t_{\mathrm{eq}}}$ via QSVT using Λ-dependent phase angles. Methods for this are discussed in the main text and circuits given in Supplementary Information 4 B. Here we illustrate the use of the standard QSVT scheme in Ref.[37], where we would load the phase angles from a separate quantum register and where an angle finding algorithm would be implemented. We ignore the LCU required to add cos and sin together, as well as amplitude amplification for simplicity. Note the CNOT gate that copied the contents of the bath register $|\bar{s}\rangle$ before it is traced out. This is due to the extended Hamiltonian with the Nosé thermostat being dependent on s and is thus required for a description of the thermal state, while still being needed to be traced out in an analog of being integrated over in classical molecular dynamics simulations. The small $|0\rangle$ on the wires indicates that the ancilla qubits are returned to the zero state after robust oblivious amplitude amplification[35] such that they can be reused as the ancilla qubits for the Hadamard test.

TABLE 1. *Overview of results on algorithmic complexity in terms of Toffoli gate count.* Here we consider the Toffoli gate count in terms of N (the number of nuclei), $\tilde{N}$ (the number of electrons), $N_{\mathrm{tot}} = N + \tilde{N}$ (the total number of particles), t (the evolution time), ε (the precision of the state preparation/free energy estimation), δ (a lower bound for the overlap between the approximate ground state prepared by an oracle U_I and the true ground state), γ (a lower bound on the spectral gap of the electronic Hamiltonian), η (the number of grid points in phase-space, which is exponential in N), and $1-\xi$ (the success probability for free energy estimation). Throughout this paper, we use the notation $\tilde{\mathcal{O}}(\cdot)$ to hide polylogarithmic factors. For simplicity in this table, we suppress the dependence on all other variables for simplicity and use the notation $\mathcal{O}^*(\cdot)$ to hide both polylogarithmic dependencies and $o(1)$ terms in the exponent. More details can be found in Supplementary Information 3. Note that in this work we compute the difference of free energies between two systems while Ref.[29] computes the absolute free energy of a single system.

	Molecular dynamics	Free energy calculation
Liouvillian + Trotterization[29]	$\mathcal{O}^*\left(\frac{N^2\tilde{N}^2N_{\mathrm{tot}}^3t}{\delta\gamma\varepsilon^{o(1)}}\right)$	$\mathcal{O}^*\left(\left(\left(\frac{\eta^{o(1)}N^2\tilde{N}^2N_{\mathrm{tot}}^3t}{\delta\gamma\,\varepsilon}\left(N_{\mathrm{tot}}^2+\frac{\eta}{\sqrt{\varepsilon}}\right)+\frac{\tilde{N}N_{\mathrm{tot}}^4}{\varepsilon^2}\right)\log\frac{1}{\xi}\right)$
Our work	$\tilde{\mathcal{O}}\left(\frac{N\tilde{N}N_{\mathrm{tot}}^3t}{\delta\gamma}\log^3\frac{1}{\varepsilon}\right)$	$\tilde{\mathcal{O}}\left(\frac{N\tilde{N}N_{\mathrm{tot}}^5t}{\delta\gamma\varepsilon}\log\frac{1}{\xi}\right)$

Algorithm 1: Quantum algorithm for Liouvillian simulation

Input: Number of nuclei N, Evolution time t, Precision ε, Block encoding of the electronic Hamiltonian $H_{\mathrm{el}}^{\mathrm{ctrl}}$[104], Block encodings of the nuclear-position-controlled electronic force operator $\partial_{x_{n,j}} H_{\mathrm{el}}^{\mathrm{ctrl}}$ for $n \in [N]$ and $j \in \{1,2,3\}$[26], Block encoding of the discretized momentum derivative operator $D_{p'_{n,j}}$ for $n \in [N]$ and $j \in \{1,2,3\}$[29], Block encoding of the classical Liouvillian L_{class}[29], Approximate ground state preparation oracle U_I, Quantum state $|\rho_0\rangle$ encoding initial phase-space density of nuclei and heat bath.

Output: ε-close approximation of $|\rho_t\rangle = e^{-iLt}|\rho_0\rangle$ in ℓ_2 distance

for *every query to the block encoding L in the QSVT-based Hamiltonian simulation algorithm*[37] **do**

- Prepare state $\frac{1}{\sqrt{3N}} \sum_{n=1}^{N} |n\rangle \otimes \sum_{j=1}^{3} |j\rangle$ and additional electronic register.
- Apply approximate ground state preparation oracle U_I to nuclear and electronic registers $U_I |\bar{\boldsymbol{x}}\rangle |0\rangle \to |\bar{\boldsymbol{x}}\rangle |\phi_{\mathrm{init}}(\boldsymbol{x})\rangle$.
- Apply ground state preparation algorithm with nuclear-position-controlled electronic Hamiltonian $H_{\mathrm{el}}^{\mathrm{ctrl}} = \sum_{\boldsymbol{x}} |\bar{\boldsymbol{x}}\rangle\langle\bar{\boldsymbol{x}}| \otimes H_{\mathrm{el}}(\boldsymbol{x})$.
- Controlled on $|n\rangle$ and $|j\rangle$, apply nuclear-position-controlled electronic force operator $\partial_{x_{n,j}} H_{\mathrm{el}}^{\mathrm{ctrl}} = \sum_{\boldsymbol{x}} |\bar{\boldsymbol{x}}\rangle\langle\bar{\boldsymbol{x}}| \otimes \frac{\partial H_{\mathrm{el}}(\boldsymbol{x})}{\partial \boldsymbol{x}_{n,j}}$.
- Uncompute the (approximate) electronic ground state to obtain block-encoding of $D_{n,j}^{\mathrm{el}}$ controlled on $|n\rangle$ and $|j\rangle$.
- Controlled on $|n\rangle$ and $|j\rangle$, tensor product $D_{n,j}^{\mathrm{el}}$ with discretized momentum derivate operator $D_{p'_{n,j}}$.
- Use LCU to sum over registers $|n\rangle$ and $|j\rangle$ to obtain block encoding of electronic Liouvillian L_{el}.
- Use LCU to sum over classical Liouvillian L_{class} and electronic Liouvillian L_{el} to obtain block encoding of Liouvillian L.

Apply e^{-iLt} operator obtained from QSVT-based Hamiltonian simulation algorithm to $|\rho_0\rangle$.

return ε-close approximation of $|\rho_t\rangle = e^{-iLt}|\rho_0\rangle$.

Algorithm 2: Quantum algorithm for thermodynamic integration

Input: Number of interpolation points N_Λ, Equilibration time t_{eq}, Precision ε, Failure rate ξ, Block encoding of Liouvillian of systems A/B over nuclear phase-space U_{L_A}/U_{L_B} and scaling factors $\alpha_{L_A}/\alpha_{L_B}$ from Proposition 2, Block encoding of the difference of the nuclear Hamiltonian between systems A and B over nuclear phase-space $U_{\Delta H}$ and scaling factor α_Δ, Initial nuclear phase-space density $|\rho_0\rangle = \sum_{\boldsymbol{x},\boldsymbol{p}',s,p_s} c_{\boldsymbol{x},\boldsymbol{p}',s,p_s} |\bar{\boldsymbol{x}}\rangle |\bar{\boldsymbol{p}}'\rangle |\bar{s}\rangle |\bar{p}_s\rangle$

Output: Helmholtz free energy difference $\Delta F_{A\to B}$ within ε additive error with success rate $1-\xi$

Prepare uniform superposition over N_Λ such that $\frac{1}{\sqrt{N_\Lambda}} \sum_{\bar{\Lambda}=0}^{N_\Lambda-1} |\Lambda\rangle$ where $\bar{\Lambda} = N_\Lambda \cdot \Lambda$.

Use quantum arithmetic circuits[60] to compute a fixed point representation of $\alpha_\Lambda = \alpha_{L_A} + \Lambda(\alpha_{L_B} - \alpha_{L_A})$ such that we have $\frac{1}{\sqrt{N_\Lambda}} \sum_{\bar{\Lambda}=0}^{N_\Lambda-1} |\Lambda\rangle |\alpha_\Lambda\rangle$.

if *QSVT-based Hamiltonian simulation*[37] **then**

  Controlled on $|\alpha_\Lambda\rangle$, compute, on a separate register, the fixed-point representation of phase angles $\{\theta_j^\Lambda\}_{j\in[\mathcal{D}]}$ for polynomial approximation of function $f_\Lambda(x) = \exp(-i\alpha_\Lambda x t_{\mathrm{eq}})$ for degree $\mathcal{D} \in \mathcal{O}(\max(\alpha_{L_A}, \alpha_{L_B}) t_{\mathrm{eq}} + \log \frac{1}{\varepsilon})$.

else if *QSP-without-angle-finding-based Hamiltonian simulation*[55] **then**

  Controlled on $|\alpha_\Lambda\rangle$, using quantum arithmetic circuits to compute $\exp(-it\alpha_\Lambda \cos \frac{2\pi k}{4\mathcal{D}})$ for $k \in [4\mathcal{D}]$ for degree $\mathcal{D} \in \mathcal{O}(\max(\alpha_{L_A}, \alpha_{L_B}) t_{\mathrm{eq}} + \log \frac{1}{\varepsilon})$.

  Use controlled rotations to create a diagonal block encoding of the values $\exp(-it\alpha_\Lambda \cos \frac{2\pi k}{4\mathcal{D}})$ for $\Lambda \in [N_\Lambda]$, $k \in [4\mathcal{D}]$.

for *every query to the block encoding L in the Hamiltonian simulation algorithm* **do**

  Use quantum arithmetic circuits to compute a fixed point representation of $\frac{(1-\Lambda)\alpha_{L_A}}{\alpha_{L_\Lambda}}$ such that we have $\frac{1}{\sqrt{N_\Lambda}} \sum_{\bar{\Lambda}=0}^{N_\Lambda-1} |\Lambda\rangle |\alpha_\Lambda\rangle \left|\frac{(1-\Lambda)\alpha_{L_A}}{\alpha_{L_\Lambda}}\right\rangle$

  Controlled on $\left|\frac{(1-\Lambda)\alpha_{L_A}}{\alpha_{L_\Lambda}}\right\rangle$, take weighted LCU to prepare block encoding of $L_\Lambda = L_A + \Lambda(L_B - L_A)$.

  Uncompute $\left|\frac{(1-\Lambda)\alpha_{L_A}}{\alpha_{L_\Lambda}}\right\rangle$.

Controlled on $|\Lambda\rangle$, obtain $e^{-iL_\Lambda t_{\mathrm{eq}}}$ from Hamiltonian simulation algorithm such that we have $\sum_{\bar{\Lambda}=0}^{N_\Lambda-1} |\Lambda\rangle\langle\Lambda| \otimes e^{-iL_\Lambda t_{\mathrm{eq}}}$.

Apply $\sum_{\bar{\Lambda}=0}^{N_\Lambda-1} |\Lambda\rangle\langle\Lambda| \otimes e^{-iL_\Lambda t_{\mathrm{eq}}}$ to $\frac{1}{\sqrt{N_\Lambda}} \sum_{\bar{\Lambda}=0}^{N_\Lambda-1} |\Lambda\rangle \otimes |\rho_0\rangle$.

Duplicate register $|\bar{s}\rangle$ using CNOTs to retain information of the bath register.

Apply the Hadamard test[32] to the block encoding of ΔH on the registers $|\bar{\boldsymbol{x}}\rangle |\bar{\boldsymbol{p}}'\rangle |\bar{s}\rangle$ to obtain amplitude $\sqrt{\frac{1}{2}(\frac{\Delta\tilde{F}}{\alpha_\Delta} + 1)}$ on $|0\rangle$ of the measurement qubit.

Use amplitude estimation[44] to obtain $\frac{1}{2}(\frac{\Delta\tilde{F}}{\alpha_\Delta} + 1)$ to $\frac{\varepsilon}{2\alpha_\Delta}$ precision with $1-\xi$ success rate.

return ε-close estimate of Helmholtz free energy difference ΔF
